UNIVERSIDADE D
COIMBRA

Beatriz Maria Gomes Oliveira

THE ROLE OF α-ADDUCIN IN THE FUNCTION AND STRUCTURE OF RETINA

Thesis submitted to the Faculty of Sciences and Technology of the University of Coimbra
for the degree of Master in Biomedical Engineering
with specialization in Biomedical Instrumentation and Biomaterials,
supervised by Dr. Elisa Regina Figueiras Julião Inácio de Campos
and Dr. António Francisco Rosa Gomes Ambrósio

September 2018

FACULDADE DE CIÊNCIAS E TECNOLOGIA
UNIVERSIDADE D COIMBRA

The role of α-adducin in the function and structure of retina

Submitted in Partial Fulfilment of the Requirements for the Degree of Master in Biomedical Engineering with the speciality of Biomedical Instrumentation and Biomaterials

Author

Beatriz Maria Gomes Oliveira

Advisors

Dr. Elisa Regina Figueiras Julião Inácio de Campos

Dr. António Francisco Rosa Gomes Ambrósio

Jury

President	Prof. Dr. Emília da Conceição Pedrosa Duarte Assistant Professor at the Department of Life Sciences of University of Coimbra
Vowels	Dr. Elisa Regina Figueiras Julião Inácio de Campos Postdoctoral Fellow (Fundação para a Ciência e Tecnologia, SFRH/BPD/93672/2013) Dr. Rosa Cristina Simões Fernandes Assistant Investigator at the Faculty of Medicine of University of Coimbra

Institutional Collaboration

iCBR Coimbra Institute for Clinical and Biomedical Research

FACULDADE DE MEDICINA UNIVERSIDADE D COIMBRA

3S INSTITUTO DE INVESTIGAÇÃO E INOVAÇÃO EM SAÚDE UNIVERSIDADE DO PORTO

Coimbra, September, 2018

This work was funded by FEDER funds through the COMPETE 2020 Programme, under the project POCI-01-0145-FEDER-007440, by National Funds through Portuguese Foundation for Science and Technology (Fundação para a Ciência e a Tecnologia, FCT) under the project PEst-UID/NEU/04539/2013, and by Centro 2020 Regional Operational Programme (BRAINHEALTH 2020 (CENTRO-01-0145-FEDER-000008)).

EC was financially supported by the FCT Postdoctoral Fellowship SFRH/BPD/93672/2013, through European Union and National funds and co-funded by Human Capital Operating Programme (Programa Operacional do Capital Humano, POCH).

“All you dreamers keep dreaming
And let those dreams rise into the light”
U Know Who I Am, David Fonseca, 2009

[Aos meus pais]

ACKNOWLEDGMENTS

À Doutora Elisa Campos, orientadora desta tese, por todo o apoio e ajuda, por todo o foco e rigor e por toda a partilha de conhecimento científico, prático e teórico, transmitido ao longo deste tempo.

Ao Doutor Francisco Ambrósio, co-orientador desta tese, por me ter aceite no seu grupo de investigação, por todo o incentivo, partilha de conhecimento e pelos recursos fornecidos.

À Doutora Mónica Sousa, colaboradora neste trabalho, pela transmissão de conhecimento e empenho.

Agradeço a todos os meus colegas de laboratório pela boa disposição, pela ajuda, pela partilha e por me terem recebido de braços abertos. Quando entrei no grupo, a minha prática laboratorial era muito reduzida e, neste momento, sinto que levo uma grande bagagem para o futuro. A todos os membros integrantes do *Tricot by Boia*, por toda a amizade e pelos momentos de descontração que foram tão importantes ao longo deste percurso. Tenho a certeza que não iremos perder o contacto! À Lia Costa, minha 'colega de tese', pela amizade, pelas gargalhadas sem fim, por todas as conversas matinais e por ter sido um apoio tão importante neste ano. Tenho a certeza que o suporte que demos uma à outra foi essencial para superar todos os obstáculos que apareceram no caminho.

Quero também agradecer aos amigos que tive a sorte de encontrar em Coimbra, ao longo destes 5 anos, e que foram essenciais neste percurso. Uma palavra especial para a Mariana: obrigada por toda a amizade, por me teres ouvido sempre, pelo incentivo e por te teres revelado uma ótima conselheira. Ritinha, por todo o carinho, por todos os momentos e pela alegria. Com vocês, ficou provado que a distância não é impedimento para nada! Não posso esquecer de agradecer à melhor 'família' que Coimbra me podia ter dado! À minha Andreia, que tem um coração de ouro, por me ter acolhido, por todos os conselhos e por se ter tornado um pilar tão grande. À minha Joaninha, de quem eu muito me orgulho, por todo o carinho, boa disposição e amizade. À minha Rute, por todos os sábios conselhos e palavras amigas.

Por último, um grande obrigado à minha família e em especial aos meus pais. Pelo suporte emocional e monetário, por toda a motivação, pelas viagens semanais Aveiro-Coimbra, por nunca me terem deixado cair, por me terem dado na cabeça quando mereci, por acreditarem sempre em mim, por todos os 'tu consegues' e pelo lema 'um dia de cada vez' que aprendi a pôr em prática e vou levar para sempre.

Fui uma sortuda por vos ter comigo ao longo do meu percurso académico. A todos, do fundo do coração, um sincero obrigada!

Abstract

Neurons are polarized and specialized cells responsible for the directional information flow in the central nervous system (CNS). Their organized cytoskeleton is composed by microtubules, neurofilaments and several proteins such as actin, spectrin and adducin. Spectrin tetramers act as spacers of actin rings, which are periodically disposed along the axon shaft. Adducin, located at the growing end of actin filaments, is an actin-binding protein encoded by three closely related genes, alpha (α), beta (β) and gamma (γ).

It is already known that adducin assumes an important role in the stabilization of the diameter of actin rings. Although it is also known that deletion of α-adducin gene (*Add1*) leads to optic nerve enlargement and consequent degeneration, the effect of this protein in the physiology and structure of the retina was not addressed, so far. Therefore, the aim of the present study was to evaluate the role of α-adducin in the function and structure of the retina.

α-adducin knockout (KO) mice were obtained from heterozygous breeding pairs. At P100, wild-type (WT) and KO animals were submitted to electroretinography (ERG) and optical coherence tomography (OCT) to assess retinal function and structure, respectively. The presence of opacities in the lens of KO animals hindered the observation of the retinal structure by OCT.

Regarding ERG, dark and light-adapted retinal light responses were recorded. It was found a significant increase (up to 25%) in the a-wave time to peak values, in the scotopic response, and in the phase of fundamental and first harmonic waves, in the photopic flicker test.

In the same time point, structural changes in about 26% of retina extension were observed in the retina of KO animals. Comparing to WT animals, KO animals presented: (i) higher density of ganglion and amacrine cells, (ii) increased length and abnormal morphology of bipolar cells, (iii) horizontal cells with different orientation and morphology, (iv) apparent worsening organization of cones, (v) higher density and reactivity of microglial cells. These characteristics were more

evident in the areas presenting structural changes. Nevertheless, no cell death by apoptosis was detected.

In conclusion, we show, for the first time, that deletion of α-adducin induces evident structural changes in the retina, namely the morphology of some retinal cells, despite subtle functional alterations.

Further studies will be important to carry out in order to assess the time point where this protein affects the retinal development, thus, explaining some features that remain unclear.

Keywords retina, adducin, cytoskeleton, neurons, neuroinflammation

Resumo

Os neurónios são células polarizadas e especializadas responsáveis pelo fluxo de informação no sistema nervoso central (SNC). O seu organizado citoesqueleto é maioritariamente composto por microtúbulos, neurofilamentos e várias proteínas, tais como a actina, a espectrina e a aducina. Os tetrâmeros de espectrina atuam como 'espaçadores' dos anéis de actina, os quais se encontram periodicamente dispostos ao longo do eixo axonal. A aducina, localizada na extremidade dos filamentos de actina nos quais ocorre a sua polimerização, é uma proteína codificada por três genes semelhantes, alfa (α), beta (β) e gama (γ).

Resultados previamente publicados demonstraram o importante papel que a aducina assume na estabilização do diâmetro dos anéis de actina. Foi também provado que a ausência do gene da α-aducina (*Add1*) provoca o alargamento do nervo ótico e consequente degenerescência. No entanto, o efeito desta proteína na fisiologia e estrutura da retina nunca foi analisado. Assim, o presente estudo teve como objetivo a avaliação do papel da α-aducina na função e estrutura da retina.

Murganhos KO para a α-aducina foram obtidos a partir de casais reprodutores heterozigóticos. Cem dias após o seu nascimento, os animais *wild type* (WT) e *knock-out* (KO) foram submetidos às técnicas de eletrorretinografia (ERG) e tomografia de coerência ótica (OCT; do inglês, optical coherence tomography) por forma a avaliar a função e estrutura da retina, respetivamente. A presença de opacidades na lente dos animais KO impediu a observação da estrutura da retina, a partir da técnica de OCT.

Relativamente à técnica de ERG, foram analisadas as respostas sob condições de escuro e de luz. Na resposta escotópica, a ausência da α-aducina resultou num aumento significativo (até 25%) do tempo de latência da onda-a. As fases da onda fundamental e da primeira harmónica também estavam significativamente aumentadas no teste *flicker* fotópico.

No mesmo ponto temporal, foram observadas alterações estruturais em 26% da extensão da retina. Comparativamente aos WT, os animais KO apresentaram: (i) uma maior densidade das células ganglionares e amácrinas, (ii) um aumento do

comprimento e morfologia invulgar das células bipolares, (iii) células horizontais com diferentes orientações e morfologias, (iv) uma aparente desorganização dos cones, (v) uma maior densidade e reatividade das células da microglia. Estas características tornaram-se ainda mais evidentes nas áreas em que se observaram alterações estruturais. Todavia, não foi detetada morte celular, pelo mecanismo de apoptose.

Sumariamente, pela primeira vez, demonstrámos que a ausência da α-aducina induz alterações estruturais evidentes na retina, nomeadamente na morfologia de algumas células, sendo a função da retina apenas subtilmente afetada.

Estudos posteriores serão importantes para avaliar o momento em que esta proteína afeta o desenvolvimento da retina, assim como explicar algumas características que ainda não permanecem claras.

Palavras-chave: retina, aducina, citoesqueleto, neurónios, neuroinflamação

Contents

LIST OF FIGURES

LIST OF TABLES

ABBREVIATIONS

AA - arachidonic acid

ABP - actin-binding protein

AJ - adherens junctions

ANOVA - analysis of variance

ALS - amyotrophic lateral sclerosis

AP2-α - activating enhancer binding protein 2-α

ARVO - Association for Research in Vision and Ophthalmology

ATP - adenosine triphosphate

BDNF - brain derived neurotrophic factor

BRB – blood-retinal barrier

Brn3a - brain-specific homeobox/POU domain protein 3A

BSA - bovine serum albumin

CCL - CC chemokine ligand

cGMP - nucleotide cyclic guanosine monophosphate

CNS - central nervous system

DAPI - 4’,6-diamidino-2-phenylindole

DTT – dithiotreitol

DIV - days in vitro

DNA - deoxyribonucleic acid

dATP - deoxyadenosine triphosphate

dUTP - deoxyuridine triphosphate

EDTA - ethylenediaminetetraacetic acid

ERG - electroretinography/electroretinogram

FFT - fast fourier transform

GABA - gamma-aminobutyric acid

GCL - ganglion cell layer

GDNF - glial cell line-derived neurotrophic factor

GFAP - glial fibrillary acidic protein

GluR - ionotropic glutamate receptors

GS - glutamine synthetase

Iba1 - calcium-binding adapter molecule 1

IBMC - Institute for Molecular and Cell Biology

IFN - interferon

IgG - immunoglobulin

IM - intramuscular injection

IN - inner segment

INL - inner nuclear layer

IOP - intra-ocular pressure

IP - intraperitoneal

IPL - inner plexiform layer

IQR - interquartile range

KO - knockout

LPS - lipopolysaccharide

LSD - least significant difference

MARCKS - myrostoykated alanine-rich C kinase substrate

mGluR - metabotropic glutamate receptors

NFL - nerve fiber layer

NO - nitric oxide

OCT - optical tomography coherence

OCT (compound) - optimal cutting temperature (compound)

ONL - outer nuclear layer

OP - oscillatory potential

OPL - outer plexiform layer

OS - outer segment

OX6, MHC-II - major histocompatibility complex 2

PBS - phosphate-buffered saline

PFA - paraformaldehyde

PKA - protein kinase A

PKC - protein kinase C

PKC-α - protein kinase C-α;

PSD95 - postsynaptic density protein 95

RGC - retinal ganglion cell

Rok - rho-associated kinase

ROS - reactive oxygen species

RPE - retinal epithelial layer

rTdT - recombinant terminal deoxynucleotidyl transferase

SEM - standard error of the mean

SD-OCT - spectral domain optical tomography coherence

SSC - saline sodium citrate

STORM - stochastic optical reconstruction microscopy

TJ - tight junctions

TNF - tumor necrosis factor

TUNEL - terminal deoxynucletidyl transferase dUTP nick-end labeling

WT - wild type

1.INTRODUCTION

1.1. The eye

The main function of the eye is to convert the incident light into electrical signals and transmit them to the brain, through the optic nerve, where the visual information is processed (Purves *et al.*, 2004; Galloway *et al.*, 2016).

The eyeball is a fluid-filled sphere that can be diverted in three regions (Figure 1.1): the outer, the middle and the inner layer corresponding to fibrous, vascular and nervous tissues, respectively (Purves *et al.*, 2004).

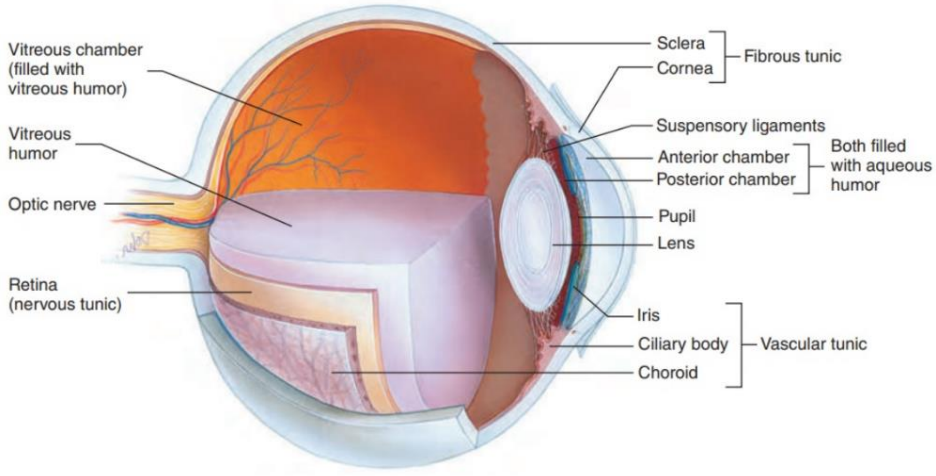

Figure 1.1. Anatomy of the eye (Adapted from http://annahamilton.me/anatomy-of-eye-lecture.html).

The outermost layer of the eye comprises the cornea and the sclera. Whereas the cornea is transparent and provides most of the focusing power of the eye, the sclera is an opaque (white) and thicker tissue which contains collagen fibers and acts as a protective barrier of the internal structures (Mitchell and Grimmer, 2013; Galloway *et al.*, 2016). The border between this two structures, cornea and sclera, is named limbus (Van Buskirk, 1989). On the other side, the middle layer, usually known as uveal tract, contains the choroid, the iris and the ciliary body (Kolb, Fernandez and Nelson, 1995). The first tissue is the largest component of this layer,

being responsible for oxygen and nutrition supply to the retina. It also contains a high concentration of melanin, essential to control the reflection process. The iris is a circular, colored and thin structure that controls the amount of light that reaches the eye, once regulates the expansion/contraction of the pupil (Kolb, Fernandez and Nelson, 1995; Purves *et al.*, 2004). The ciliary body is a circumferential tissue, composed by ciliary muscles and ciliary processes, which assumes an important role in the accommodation reflex by enabling the change of the lens shape. The ciliary processes also produce aqueous humor, the fluid that that occupies the anterior and posterior chambers of the eye (Purves *et al.*, 2004; Mitchell and Grimmer, 2013). Last of all, the retina defines the innermost layer of the eye. The structure and function of the retina will be described later in this chapter.

Besides the previous structures, the eye comprises also particular compartments known as chambers (Galloway et al., 2016). In the path between cornea and retina, the light passes through three different fluid compartments.

The cornea and the lens limit the anterior chamber. The anterior chamber is filled with aqueous humor, a solution of water and electrolytes, which provides oxygen and nutrients to eye tissues, removes their waste products and helps to maintain a constant pressure inside the eye. For the pressure to remain constant, its production must be balanced by its drainage (elimination) (Siggers and Ethier, 2012). The aqueous humor leaves the eye by passive flow, primarily, through a conventional pathway in which are involved the trabecular meshwork and the Schlemm's canal, a vascular structure. However, a small portion passes through an unconventional route that includes the ciliary muscle, supraciliary and suprachoroidal spaces. In the two pathways, the fluid is released into the systemic circulation (Goel *et al.*, 2010; Johnson, McLaren and Overby, 2017).

A disruption of the aqueous flow leads to an elevation of the intra-ocular pressure (IOP), a condition associated with glaucoma (Kolb, Fernandez and Nelson, 1995; Galloway *et al.*, 2016). As said before, the aqueous humor is produced by the ciliary processes and its access to the anterior chamber is regulated by the pupil (Galloway *et al.*, 2016; Snytnikova *et al.*, 2017). Finally, the vitreous chamber is located between the lens and the retina, and it represents 80% of the total volume of the eye. This chamber is filled by the vitreous humor, which is predominantly composed by water (>98%), collagen and polymerized hyaluronic acid. The vitreous

chamber contributes to maintain the spherical shape of the eye and the intraocular pressure, helping to keep the retina in the right place. In addition, the vitreous humor also contributes to an efficient light transmission due to the activity of specific phagocytic cells that allow the removal of blood and other debris (Purves *et al.*, 2004; Siggers and Ethier, 2012).

1.2. The retina

The retina is located in the innermost layer of the eye and is composed by seven different layers (Figure 1.2). It is known as part of Central Nervous System (CNS) since it is derived from the embryonic forebrain. Also, about 80% of the sensory information, in humans, is formed in the retina (Cole, 1982; Hildebrand and Fielder, 2011).

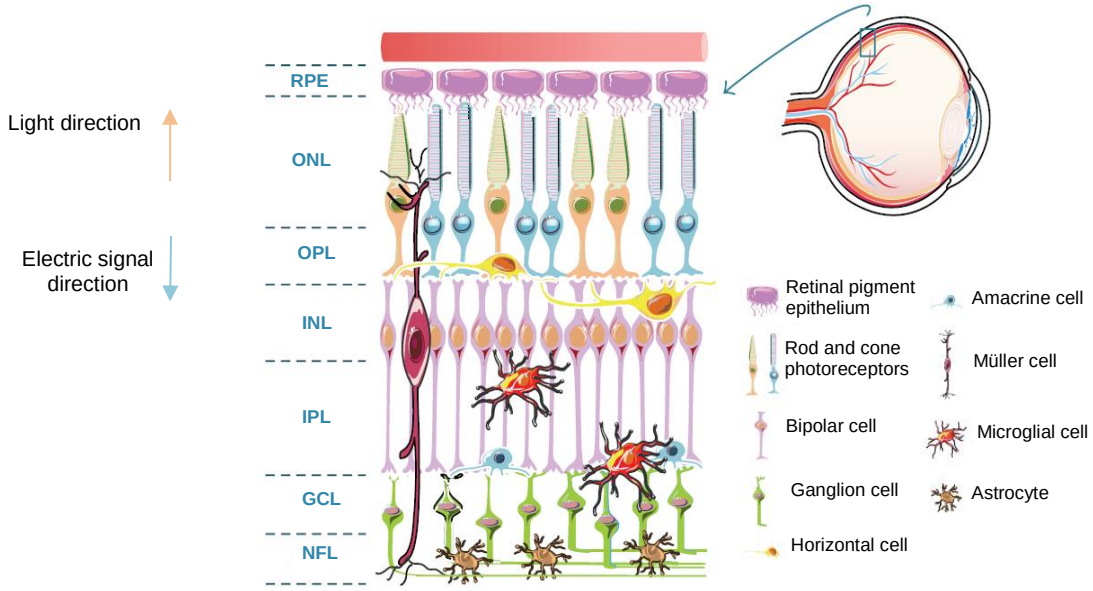

Figure 1.2. Schematic representation of retinal cells, layers, paths of the light and electrical signals. The neuronal retina is composed by rod and cone photoreceptors, bipolar, ganglion, horizontal and amacrine cells. In addition, the retina also contains glial cells such as astrocytes, Müller and microglial cells. RPE: retinal pigmented epithelium; ONL: outer nuclear layer; OPL: outer plexiform layer; INL: inner nuclear layer; IPL: inner plexiform layer; GCL: ganglion cell layer; NFL: nerve fiber layer (Adapted from Madeira *et al.*, 2015).

The retina is composed by three neuronal nuclear layers and two plexiform (synaptic) layers. The outer nuclear layer (ONL) contains the cell body of the photoreceptors. The cell body of the bipolar, horizontal and amacrine cell are located in the inner nuclear layer (INL). The ganglion cell layer (GCL) includes the cell body of the retinal ganglion cells (RGCs) and displaced amacrine cells (Madeira *et al.*, 2015). These cells interact with each other in the plexiform layers: in the outer plexiform layer (OPL) occurs the synapses between photoreceptors and bipolar and horizontal cells, whereas the bipolar cells synapse with RGCs and amacrine cells in the inner plexiform layer (IPL) (Schiller, 2010; Madeira *et al.*, 2015).

The neurons are involved in the phototransduction process. Briefly, they respond to a light stimulus and produce an electric signal that travels, via the optic nerve to the brain, where it is processed, creating the visual perception (Melloni, 1971).

However, when the light reaches the eye, the retina is not the first layer encountered. Due to the vital molecule for photoreceptor pigment-bearing membranes, vitamin A, be provided by the retinal epithelial layer (RPE), the photoreceptors must be in contact with this structure. Therefore, the light should pass through all the retina until reach photoreceptors surface, where is produced the corresponding electrical signal. Subsequently, it needs to travel back to the outermost layer of the retina (Melloni, 1971), as is schematized in Figure 1.2.

The RPE consists on a monolayer of non-divided cells that have a high density of melanin. This pigment is essential to prevent the reflection of stray photons, by absorbing them, and to protect retinal cells from an excessive light radiation (Melloni, 1971; Cunha-Vaz, 2004; Cholkar *et al.*, 2013).

The blood-retinal barrier (BRB) is a restrictive physiological barrier that consists of two anatomical components, an inner BRB (iBRB) and an outer BRB (oBRB). Whereas the oBRB is composed by tight (TJ) between RPE cells, the iBRB is formed by TJ between retinal capillary endothelial cells and its activity can be influenced by astrocytes, Müller cells and pericytes. The presence of this barrier is essential to regulate the fluid and molecular movements into and out of the retina (Cunha-Vaz, 2004, 2009).

The retina also contains epithelial and glial cells (Madeira *et al.*, 2015). Particularly, glial cells are essential to retinal homeostasis and do not have a specific

localization, unlike the neuronal cells. Müller cells, the most abundant glial type, span all over the retina, whereas microglia cells are mainly disposed in IPL and GCL (in a non-activated state). The astrocytes are present in the NFL, the layer where the axons of the RGCs forming the optic nerve can be found (Fernández-Sánchez *et al.*, 2015; Vecino *et al.*, 2016).

1.2.1. The neuronal retina

1.2.1.1. Retinal ganglion cells

The RGCs are the final output neurons in the retina. RGCs can be diverted in ON and OFF-center cells (Figure 1.3), being the number of each type the same, approximately (Erisir *et al.*, 1999; Purves *et al.*, 2004) .

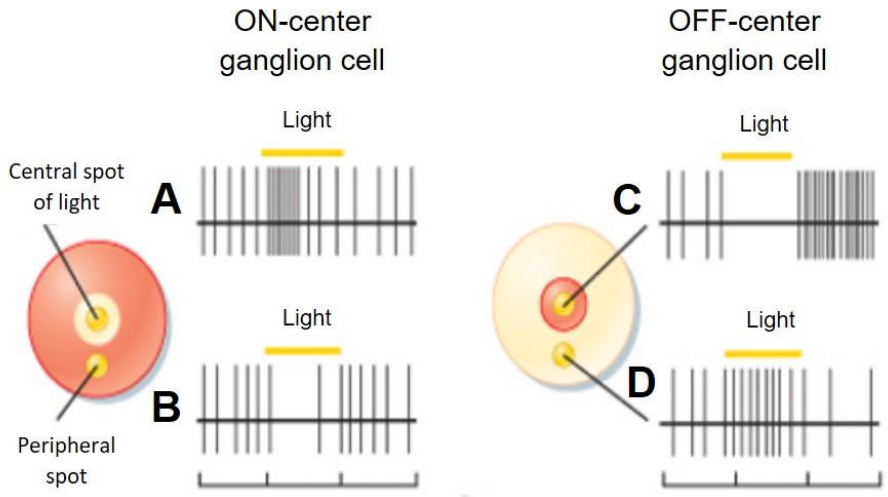

Figure 1.3. Receptive fields of ON and OFF retinal ganglion cells. ON-ganglion cells increase the rate of discharge when the receptive field center is stimulated by light (**A**), whereas a stimulation of the center-surround reduces the frequency (**B**). OFF-ganglion cells are inhibited by a spot of light on the center of its receptive field (**C**) and are stimulated when the surround is exposed to light (**D**) (Adapted from Squire, Berg and Bloom, 2012).

ON-center ganglion cells depolarize (discharge vigorously) when there is an increase of illumination in the receptive field center. On the other side, when the surround of the receptive field is exposed to light, the cells hyperpolarize. OFF-center ganglion cells discharge when the surround is exposed to light and become inactive when the center is stimulated (Squire, Berg and Bloom, 2012). ON and OFF

RGCs receive information from ON and OFF bipolar cells, respectively (Schiller, 2010).

They contact directly with amacrine and bipolar cells and indirectly with photoreceptors and horizontal cells (via the bipolar cells). Conversely to photoreceptors, bipolar, horizontal and many amacrine cells, which release neurotransmitters, RGCs communicate with other cells via action potentials (Kolb, Fernandez and Nelson, 1995). This means that, during the light stimulus, a high frequency spiking is maintained. Further, they transmit the visual signals through axons to the brain, via optic nerve, which is the bundling of the axons of RCGs (Hernandez *et al.*, 2009; Weber and Langmann, 2013). The damage of the optic nerve and gradual loss of RGCs is known to be implicated in several ocular pathologies, such as glaucoma (Santiago *et al.*, 2014).

1.2.1.2. Amacrine cells

The amacrine cells are found in the INL, but also in the IPL and in the GCL (named displaced amacrine cells) (Provis *et al.*, 2005; Lechner, O'Leary and Stitt, 2017). Almost 42 different amacrine cell types can be distinguished, which makes them the most diverse class in the retina (Euler *et al.*, 2014). These cells are interneurons without axons, thus, enabling the lateral interaction between bipolar cells and RGCs (Figure 1.4) and also between bipolar and other amacrine cells (MacNeil and Masland, 1998; Johansson, Eftekhari and Warfvinge, 2010) .

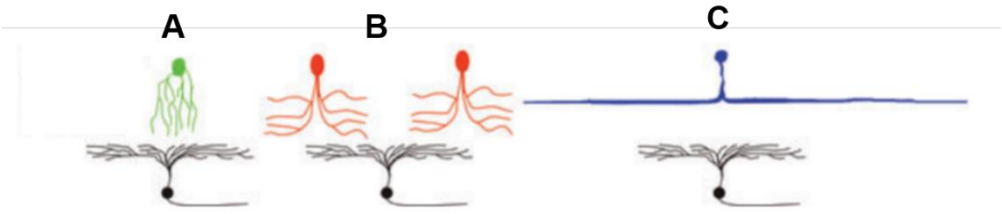

Figure 1.4. Amacrine-RGCs pathway, showing the morphology of the cells. Small-field amacrine cells (**A**) induce local glycinergic inhibition and medium field amacrine cells (**B**) generate GABAergic inhibition, extending beyond the dendrites of RGCs (represented in (black). Wide field amacrine cells (**C**), whose processes can extend over distances greater than 1mm, use GABA molecules (Adapted from Werblin, 2011).

Small and medium field amacrine cells communicate locally and use glycine and gamma-aminobutyric acid (GABA), as neurotransmitter, respectively. The processes of wide field amacrine cells project along longer distances, with the involvement of GABA molecules.

Some amacrine cells contain a reciprocal synapse, in which they synapse back on the axon terminal of bipolar cells. When bipolar cells increase the glutamate release, amacrine cells also increase the release of their neurotransmitter. At the same time, bipolar cells can communicate directly with RGCs, increasing the firing rate of RGCs. But, once GABA and glycine are inhibitory neurotransmitters, bipolar cells (due to the reciprocal synapse) are placed in a more hyperpolarized level. Then, the global effect is a reduction of the action potentials generated by the RGCs (Masland, 2012).

1.2.1.3. Bipolar cells

Bipolar cells, whose axons terminals synapse with amacrine and RGCs in the IPL, are a class of excitatory neurons characterized by graded potentials. These cells can be diverted in two types: ON and OFF bipolar cells, according to the expressed type of glutamate receptor (Figure 1.5).

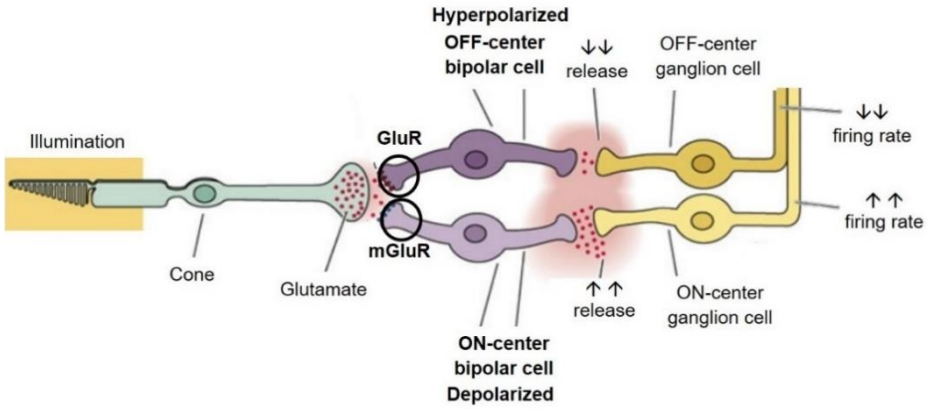

Figure 1.5. Cone – bipolar – ganglion cell path. When light interacts with the eye, cones hyperpolarize and decrease, at the synapse, the glutamate release. ON-center bipolar cells (through mGluR receptor) increase the transmitter release leading to a higher firing rate of ON-center ganglion cells. In turn, OFF-center bipolar cells (through GluR receptors) decrease the transmitter release and subsequently the firing rate of OFF-ganglion cells (Adapted from Watson and Breedlove, 2012).

ON bipolar cells express metabotropic glutamate receptors (mGluR) and act with the involvement of secondary messengers. Instead, OFF bipolar cells express ionotropic glutamate receptors (GluR), allowing or not the movement of ions through the membrane (Purves *et al.*, 2004; Xiong *et al.*, 2015; Puller *et al.*, 2017).

In response to light stimulus, ON bipolar cells depolarize, producing a *burst* of graded potentials, unlike OFF bipolar cells, that reduce the rate of discharge (Euler *et al.*, 2014). If the light hits the surround, the response in ON and OFF bipolar cells will be opposite (*cf.* Figure 1.3).

Depending on the source of the input, bipolar cells can also be classified as rod and cone bipolar cells. Rod bipolar cells receive input from until 70 rods, whereas cone bipolar cells interact with as few as one cone (Hildebrand and Fielder, 2011; Xiong *et al.*, 2015).

1.2.1.4. Horizontal cells

The horizontal cells, located in the INL, enable the lateral interaction between photoreceptors and bipolar cells, assuming, thus, the role of interneurons (Johansson, Eftekhari and Warfvinge, 2010). This cell path is totally different to the photoreceptor-bipolar cell-ganglion cell path, a vertical route that is, actually, the most direct route for transmitting information to the brain (Purves et al., 2004).

The inhibitory neurotransmitter GABA enables the horizontal cells to sharpen the response between two nearby stimuli, enhancing the differences between light and darkness (contrast enhancement), in a process known as lateral inhibition (Liu *et al.*, 2013; Kemmler *et al.*, 2014) (reviewed in Thoreson and Mangel, 2012).

Finally, in the vertebrate retinas, there are two types of horizontal cells: B-type, which are provided of axons; and A-type, which are axonless (Kolb, Fernandez and Nelson, 1995; Fitzgibbon, 1997).

1.2.1.5. Photoreceptors

The photoreceptor cells include cones and rods (Figure 1.6).

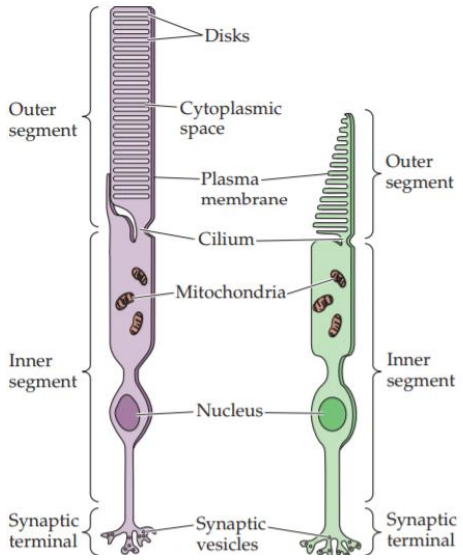

Figure 1.6. Illustrative scheme of the structure of rods and cones. Note the differences in shape, size and the arrangement of the membranous disks in the outer segments (OS) (Adapted from Purves *et al.*, 2004).

The human retina has approximately 4-5 million of cones and 77-107 million rods, the most abundant type of retinal cells. Whereas the cones are specialized in daylight vision, the rods mediate low-light vision (Kolb, Fernandez and Nelson, 1995; Ebrahimi *et al.*, 2014). However, the pattern of photoreceptors distribution is not uniform. In the fovea, at the center of the retina, the number of cones increases and becomes higher than rods. Furthermore, in the foveola, a 350 µm depression at the center of fovea and the retinal region of greatest acuity, does not contain any rod (Purves *et al.*, 2004; Hildebrand and Fielder, 2011; DuVal and Allison, 2017).

In addition to its distribution in the retina, the two types of photoreceptors are distinguished by size, shape, the type of photopigment involved in the structure, and also the pattern of synaptic connections. Both cones and rods contain structures oriented toward the RPE: the inner segment (IS), containing the cell nucleus and mitochondria, synaptic terminals, where the interaction with bipolar and horizontal

cells occurs, and the outer segment (OS) where light-sensitive photopigments are located (Purves *et al.*, 2004; Johansson, Eftekhari and Warfvinge, 2010).

There is only one type of rods but in cones three types can be distinguished: S-, M- and L-cones which are sensitive to short, medium and long wavelength lights, respectively. Rod photoreceptors contain only one type of photopigment, rhodopsin. In contrast, cone photoreceptors contain three different types of photopigments, photopsins, each one specific for each type of cone photoreceptors (Kolb, Fernandez and Nelson, 1995).

It is the light sensitive photopigment of the photoreceptors that enable the response to light, resulting in an electric signal, in a process known as phototransduction. The photopigments are composed by an apoprotein (opsin) and a covalently attached chromophore derived from vitamin A (11-cis retinal).

Briefly, in the dark, photoreceptors membrane is depolarized, thus, its terminals are continually releasing glutamate. However, when an increase in light intensity is observed, rod and cone photoreceptors hyperpolarize at around -60 mV. In this situation, the low levels of the nucleotide cyclic guanosine monophosphate (cGMP) permits few Ca^{2+} channels to open, resulting in low levels of intracellular Ca^{2+}. Then, photoreceptors hyperpolarize and reduce, at the synapse, the rate of glutamate release, the neurotransmitter involved in the vertical pathway through the retina. (Kolb, Fernandez and Nelson, 1995; Xiong *et al.*, 2015).

1.2.2. Retinal glial cells

Glial cells represent more than 90% of the CNS. Despite these cells are not directly involved in synaptic interactions and electrical signals, they provide protective and supportive functions which are helpful to define synaptic contacts, repair damaged neural tissue and provide metabolic functions for neurons (Purves *et al.*, 2004; Greter and Merad, 2013). There are three glial cell types, in the retina: Müller cells, astrocytes and microglial cells.

1.2.2.1. Müller cells

The Müller cells, whose cell bodies sit in the INL, project irregularly thick and thin processes through all the retina (Newman and Reichenbach, 1996). They occupy a strategic position in the light path: from the vitreous (where the eye receives the light) to the outer limiting membrane (where the inner segments of photoreceptor cells that receive the light are located). The Müller cells regulate extracellular concentrations of potassium, by increasing its levels upon light stimulation, and remove neurotransmitters (*e.g.*, glutamate) from extracellular space, following their release into the synapse (Newman and Reichenbach, 1996; Franze *et al.*, 2007).

It is known that inflammation leads to retinal gliosis, a process characterized by hypertrophy, proliferation, up-regulation of intermediate filament expression (*e.g.*, GFAP and vimentin), and decreased expression of glutamine synthetase (GS) (Bringmann *et al.*, 2006).

1.2.2.2. Astrocytes

The astrocytes are the most abundant glial cell type. Found within the GCL and the NFL, they contain glycogen granules and are involved in axon guidance, synaptic support, development and functioning of blood flow, and in the formation of the BRB (Kolb, Fernandez and Nelson, 1995; Newman, 2010).

In response to insults to CNS, these cells proliferate, change their morphology and increase the expression of GFAP, in a process known as astrogliosis (Kolb, Fernandez and Nelson, 1995; Newman, 2010; Coorey *et al.*, 2012; Kur, Newman and Chan-Ling, 2012; Klaassen, Van Noorden and Schlingemann, 2013).

1.2.2.3. Microglia

Described in 1919, by Cajal, as the ‘third element’, microglial cells are part of the reticuloendothelial system and are the resident phagocyte population of the CNS, accounting for 10% of the adult glial cell population in the normal brain (Graeber and Streit, 1990; Kreutzberg, 1996; Wu, 2010; Hildebrand and Fielder, 2011; Greter and Merad, 2013).

In healthy conditions, microglial cells are distributed in the plexiform layers, GCL and NFL and present a ramified morphology, extending long thin processes. In this condition, microglial cells are essential for the homeostasis of the retina, through its interaction with neurons and the other glial cells (Madeira *et al.*, 2015).

In response to an insult and/or substances released by damaged CNS cells, such as microbial agents (*e.g.*, lipopolysaccharides (LPS)) (Hetier *et al.*, 1988), pathological proteins (*e.g.*, β-amyloid) (Rogers *et al.*, 2002), adenosine triphosphate (ATP) (Kettenmann, Banati and Walz, 1993) and serum factors (*e.g.*, thrombin) (Weinstein *et al.*, 2005), microglial cells become activated. This particular stage is characterized by long-term changes in gene expression, phagocytic activity (Streit, 2002) and secretion of other signals such as (Figure 1.7) (reviewed in Block and Hong, 2005):

- Cytokines (immunomodulatory peptides) like interleukins, interferons (IFNs), tumor necrosis factor- α (TNF-α). These peptides are the first to be released in response to inflammation (Kim and de Vellis, 2005; Franze *et al.*, 2007; Tremblay and Sierra, 2014);
- Chemokines (peptide chemoattractant peptides) involving CC chemokine ligands (CCL) family (Hanisch, 2002);
- Trophic factors like glial cell line-derived neurotrophic factor (GDNF), brain derived neurotrophic factor (BDNF), essential to promote neuronal survival (Presta *et al.*, 1995);
- Small lipid inflammatory mediators, that includes derivatives of arachidonic acid (AA) and prostaglandins (Minghetti and Levi, 1998; Bhatia *et al.*, 2016).

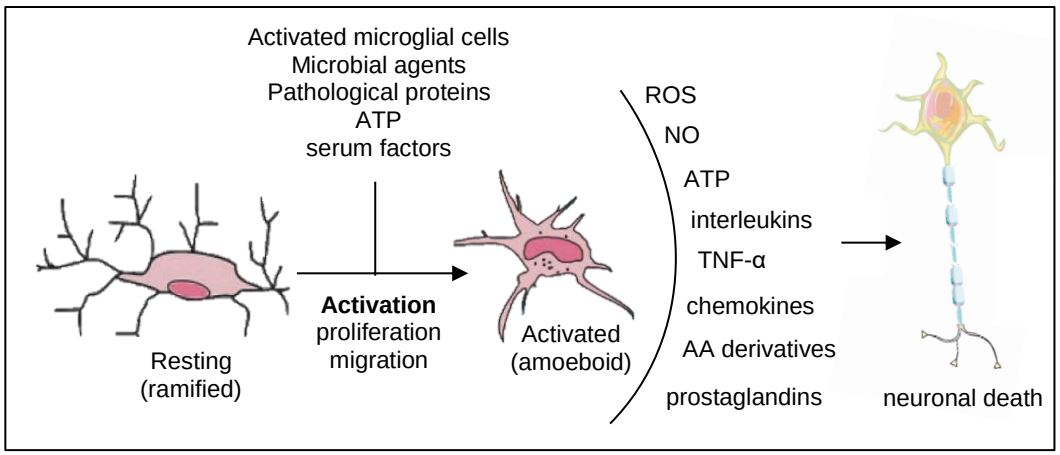

Figure 1.7. Legend on the next page.

Figure 1.7. Mechanisms involved in microglial activation, during neuronal degeneration. In the resting state, microglia present a ramified structure. Upon activation, microglia modified its structure to an ameboid shape and secrete bioactive molecules and pro-inflammatory factors.

In addition, microglial cells also release reactive oxygen species (ROS), nitric oxide (NO) and ATP (Hanisch, 2002; Santiago et al., 2014; Gao et al., 2015; Bhatia et al., 2016). In the activation process, in addition to the release of substances and proliferation, they migrate throughout the retina to the site of insult, where they alter their morphology (from ramified to amoeboid shape) (Figure 1.8) (Völgyl, Chheda and Bloomfield, 2009; Wu, 2010).

The release of inflammatory mediators contributes to the recruitment of more microglia to the lesion site and promotes the infiltration of immunomodulatory cells from the peripheral blood. Also, activated microglia can have a direct role in the promotion of astrocytic activation due to the release of pro-inflammatory markers, namely IL-1, during the inflammation process (Garden and Möller, 2006; Liu, Tang and Feng, 2011). These events have been related to CNS disorders, such as Alzheimer's and Parkinson's diseases and multiple sclerosis (Block and Hong, 2005). Besides, activation of microglial cells has been showed to precede retinal degeneration and photoreceptors apoptosis (Zeiss and Johnson, 2004; Zeng *et al.*, 2005; Gehrig *et al.*, 2007).

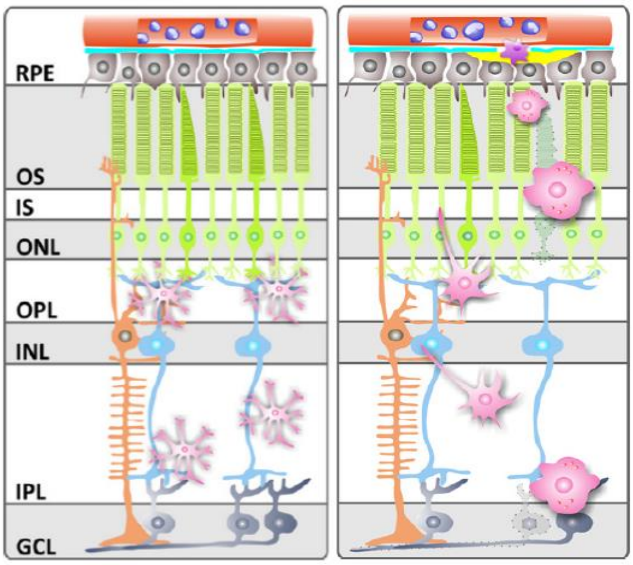

Figure 1.8. Legend on the next page.

Figure 1.8. Illustrative scheme of microglia (represented in pink) location and shape in homeostasis (left) and in an inflammatory condition (right). In the normal retina, microglial cells are limited to the plexiform layers. Different insults lead to the migration of microglial cells to lesion sites (Adapted from Karlstetter, Ebert and Langmann, 2010).

1.2.3. Retinal Histogenesis

In the retina, neurons and glial cells differentiate in a conserved order, from a pool of multipotent retinal progenitor cells (RPCs). The earliest cell types start to differentiate still in an embryonic phase (Figure 1.9), in which RGCs, horizontal cells, cones and amacrine cells are included.

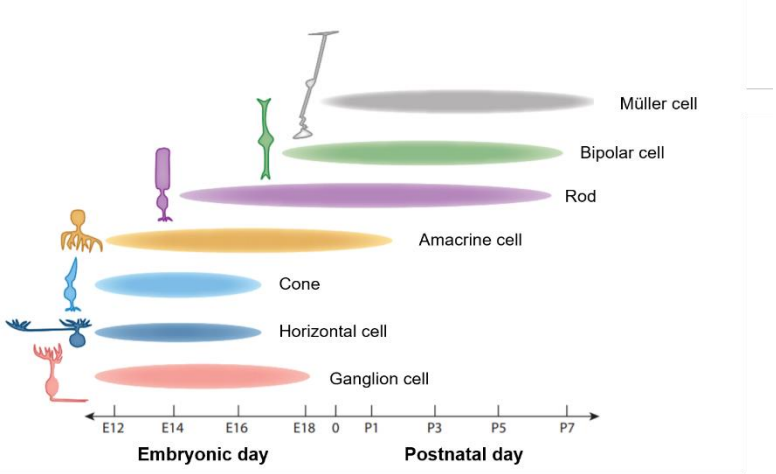

Figure 1.9. Illustrative scheme showing the sequence of retinal cells appearance and assembly, in the vertebrate retina (based on mouse development) (Cepko, 2015).

When RGCs and amacrine cells are formed, they constitute the first functional circuits in the IPL (Morgan and Wong, 2007). Next, rods differentiate and, together with cones, they contact with horizontal cells, forming the functional circuits in the OPL. Despite, in most species, cones appear before rods, their genesis can overlap (Cepko, 2015). Bipolar cells are the last neuronal population to be formed, enabling the connections between the inner and the outer retina.

The development of glial cells starts only when the retina assumes a more complex organization and requires structural, nutritional, metabolic and trophic support. Despite this sequence being conserved among species, the time between events varies (Cepko, 2014).

1.3. The axonal cytoskeleton

1.3.1. Neuronal actin rings

The neurons are polarized and specialized cells responsible for the directional information flow in the CNS. This function deeply relies on neuron asymmetry: a cell body, called the soma, with various projections (dendritic spines) that receives synaptic inputs, and an axon that transmits the information to the neighboring neurons, through the propagation of action potentials (Kapitein and Hoogenraad, 2011; Stewart and Shen, 2015).

As axons can have high length and undergo high mechanical stress, it seems plausible that they are formed by specialized architectural elements to support their structure (Roy, 2016).

The organized neuronal cytoskeleton is composed by microtubules, neurofilaments, and several proteins. It supports the lipid bilayer membrane of a eukaryotic cell, playing an important role in neuronal development, function, and structure maintenance (Stiess and Bradke, 2010; Flynn, 2013; Gallo, 2013; Zhong *et al.*, 2014). Among the proteins that are part of the cytoskeleton are actin, spectrin and adducin. The periodic cytoskeleton is only present in regions which have high content in βII spectrin, as is the case of axons. Concerning dendrites, they contain less βII spectrin quantities and do not support the growth of this assembly, being mainly composed by long actin filaments (Xu, Zhong and Zhuang, 2013; Zhong *et al.*, 2014; Coles and Bradke, 2015).

In axons, actin is disposed in short filaments and forms ring-like structures, around its circumference, with a periodicity of 180-190 nm, approximately, being colocalized with adducin, an actin-capping protein. This periodic structure starts in the proximal axon and reaches all the axon extension, from 10 days onward. Using stochastic optical reconstruction microscopy (STORM), it was demonstrated that spectrin tetramers, composed by βII and αII heterodimers, are present between adjacent actin-adducin rings aligned longitudinally along the axonal shaft (Figure 1.10), acting as a spacer (in fact, spectrin length is equal to the periodicity of actin rings). Besides contributing to the periodicity of actin rings, spectrin also assumes

an important role in the mechanical resistance of axons (Hammarlund, Jorgensen and Bastiani, 2007; Xu, Zhong and Zhuang, 2013; Lukinavičius *et al.*, 2014; Zhong *et al.*, 2014).

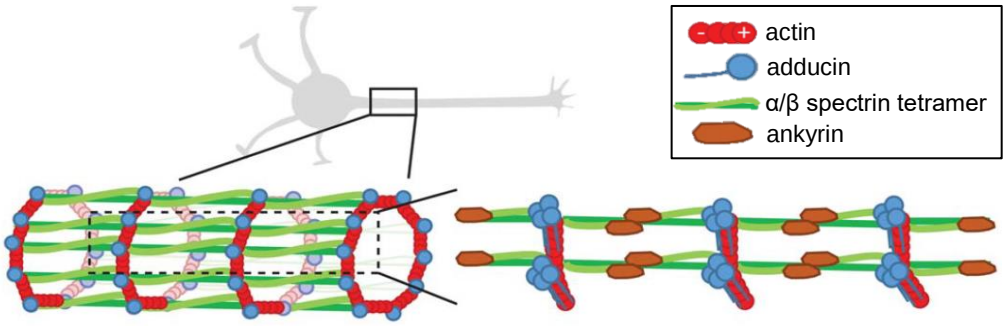

Figure 1.10. Axonal membrane organization and associated proteins. Neuron cytoskeleton is composed by actin rings that surround the axonal circumference. These rings are co-localized with adducin filaments and assume a periodicity pattern due to the presence of spectrin tetramers along the axonal shaft (Adapted from Leite and Sousa, 2016).

Along axons, other proteins can be detected such as ankyrin and protein 4.1, which have affinity for spectrin and promote the link between spectrin and the plasma membrane (Naydenov and Ivanov, 2011).

1.3.2. Adducin

1.3.2.1. Characteristics and functions

Adducin, from the greek *adducere* meaning 'to pull together', was first described in human erythrocytes, based on calmodulin binding activity (Gardner and Bennett, 1986). In mammalian cells, this protein is comprised by three closely related genes: *ADD1*, *ADD2* and *ADD3*, leading to α-, β-, γ-adducin with 726, 713 and 674 amino acids, respectively (Joshi *et al.*, 1991; Dong *et al.*, 1995; Kuhlman *et al.*, 1996). The expression of the β isoform is limited to erythrocytes and brain, whereas the α and γ ones are uniformly expressed in various tissues (Matsuoka, Li and Bennett, 2000).

Despite the differences, the three isoforms share the same organization: a N-terminal globular domain, a neck domain, and a protease-sensitive tail domain

(Figure 1.11). The end of the last domain is composed by a 22-residue myrostoykated alanine-rich C kinase substrate (MARCKS) domain, essential for the binding of adducin to spectrin-actin complexes (Joshi *et al.*, 1991; Hughes and Bennett, 1995; Li and Bennett, 1995).

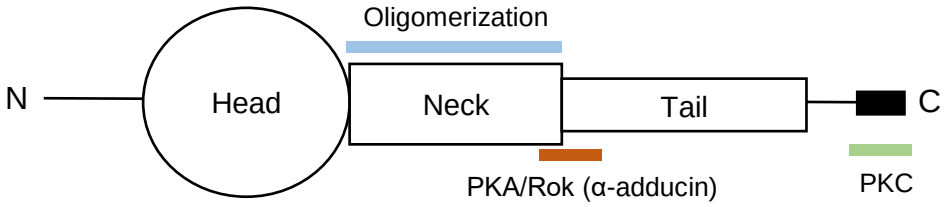

Figure 1.11. The adducin monomer. The three isoforms present the same structure: head, neck and tail domain. Oligomerization takes place in the neck domain (blue). The phosphorylation sites of protein kinase A (PKA) and Rho-associated kinase (Rok) (orange) in α-adducin, are mainly contained in the region crossing neck and tail domain whereas the MARCKS domain (solid box) binds calmodulin and contains the major phosphorylation sites of protein kinase C (PKC) (green) (Adapted from Matsuoka, Li and Bennett, 2000).

In vitro, it was demonstrated that during the neuronal maturation process, adducin displays a periodic organization only after 7 days *in vitro* (DIV7), enabling the stabilization of the structure. Thus, the actin-spectrin lattice is assumed to have a pro-stabilizer effect (Xu, Zhong and Zhuang, 2013; Zhong *et al.*, 2014).

Former studies carried out in cells showed the absence of monomeric adducin (Gardner and Bennett, 1986; Li, Matsuoka and Bennett, 1997). Therefore, it is seems that oligomerization is necessary for the functioning of adducin and takes place mainly in the neck domain, resulting in α/β and α/γ heterodimers and α/β combinations of subunits (Dong *et al.*, 1995; Li, Matsuoka and Bennett, 1997).

Adducin acts as an actin-binding protein (ABP) localized at the barbed (growing) ends of actin filaments. It also acts as a regulator of the cytoskeleton. Actually, adducin promotes the binding between actin filaments, inhibits the incorporation of new actin monomers and promotes the recruitment of spectrin to actin filaments (Kuhlman *et al.*, 1996; Matsuoka, Hughes and Bennett, 1996; Bennett and Baines, 2001).

Adducin is involved in the establishment of adherens junctions (AJ) and TJ, regulators of epithelial and endothelial cell adhesion. It was reported that the

endothelial barrier breakdown induced by LPS was associated with the loss of α-adducin from cell junctions (Naydenov and Ivanov, 2011; Kugelmann, Waschke and Radeva, 2015). This ABP is also related to the inhibition of actin-activated ATP activity of myosin subfragment-1 (S1), suggesting a role in the motility of the cell (Li and Bennett, 1995). Finally, some evidences have shown that adducin is an important molecule in synapse formation, since its deletion resulted in synapse formation impairment, in mouse and fly mutants (Bednarek and Caroni, 2011; Pielage *et al.*, 2011).

1.3.2.2. Regulation

Adducin activity can be regulated by phosphorylation through protein kinase A (PKA), protein kinase C (PKC) and Rho-associated kinase (Rok), in the neck and tail domain, preferentially, at the serine/tyrosine residues (Matsuoka, Li and Bennett, 2000).

The phosphorylation of adducin by PKC occurs mainly in the C-terminal MARCKS domain, at several serine residues. It was showed that this modification impairs adducin function, namely actin-capping and spectrin-recruiting. In fact, phosphorylation of adducin by PKC decreases its association with actin and spectrin, exposing the free barbed ends of actin filaments (Fowler *et al.*, 1998; Matsuoka, Li and Bennett, 1998). The phosphorylation by PKA has the same effect on adducin function. Concerning Rho-kinase phosphorylation, it was shown that it enhances adducin-actin interactions (Fukata *et al.*, 1999).

1.3.2.3. Influence of adducin in actin rings

The actin filaments (F-actin) are formed from globular actin (G-actin) and its polymerization occurs at the barbed ends, close to the cell membrane, while monomers are dissociated on the opposite site, the pointed end (Figure 1.12) (Campellone and Welch, 2010). These processes occur constantly once the interaction between the actin monomers are very weak (Letourneau, 2009).

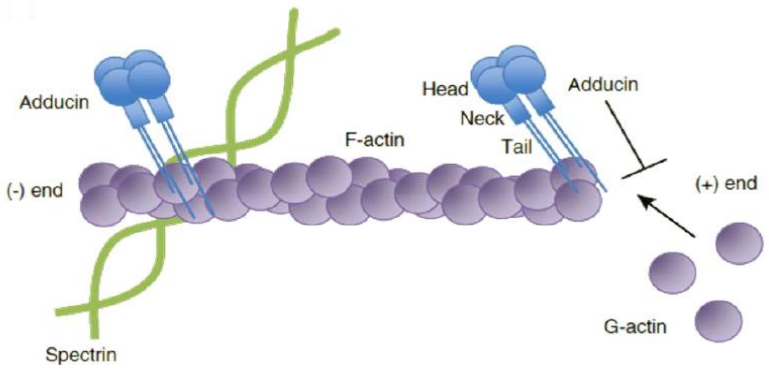

Figure 1.12. Schematic representation of adducin, actin and spectrin. Adducin is co-localized with actin (F-actin) and caps its growing ends, preventing the addition of monomeric G-actin (Adapted from Stevens and Littleton, 2011).

Adducin can associate with actin, independently from spectrin, with a high capacity but with a low affinity binding. In fact, loss of adducin was shown to impair formation of the spectrin lattice, in the plasma membrane (Naydenov and Ivanov, 2011).

Recently, it was showed that deletion of α-adducin lead to actin rings with an increased diameter, resulting in progressive axon enlargement and consequent degeneration, in the optic nerve and spinal cord of α-adducin knockout (KO) littermates (Leite *et al.*, 2016). In fact, once adducin is located at actin-spectrin junctions, its deletion will expose the barbed ends of adducin, allowing the polymerization of actin monomers and, consequently, the ring diameter increases.

It has also been reported that the dynamic growth of actin filaments promotes new synapse formation and, therefore, loss of adducin may cause changes in synapses, causing memory and learning deficits, for instance (Pielage *et al.*, 2011).

1.3.2.4. Associated diseases

Adducin has been related with several pathological conditions. Mutations in α-adducin lead to hypertension in human and in Milan hypertensive rats, an animal model of primary hypertension. Moreover, this condition impairs ion transport, due to an increase in Na^+/K^+ pump activity (Torielli *et al.*, 2008).

However, the bulk of the implicated diseases is associated with the CNS. It was showed that loss of α-adducin impairs short and long-term memory, due to its involvement in the regulation of synaptic strength and plasticity, thus, in the neuropsychological performance (Vukojevic *et al.*, 2012; Bosia *et al.*, 2016). In fact, during a degenerative process, axon enlargement (swelling) precedes axonal break and, consequently, axon loss. This situation may be related to the disruption of the periodic organization of the cytoskeleton, such as microtubules disorganization and abnormal levels of the associated proteins.

Once impairs axonal transport, outgrowth and synapse formation, the disruption of the axonal cytoskeleton has been related to neurological disorders such as amyotrophic lateral sclerosis (ALS) and Alzheimer's disease (McMurray, 2000; Robberecht and Philips, 2013).

Interestingly, in ALS patients and in a mouse model of the disease, elevated levels of phosphorylated adducin, in the spinal cord, have been reported due to the action of PKC, meaning that adducin functions were impaired. Thereby, one possibility to prevent this situation is to dephosphorylate or inhibit the phosphorylation of adducin (by PKC or PKA) which could reinforce the pre- and post-synaptic contacts (Hu *et al.*, 2003; Shan *et al.*, 2005).

OBJECTIVES

The deletion of α-adducin has been related to alterations in the neuronal development and neurodegeneration. Schizophrenia and ALS are examples of diseases associated with this protein, due to its influence on the neuronal cytoskeleton. Once retina is part of CNS and no literature has addressed the impact of α-adducin in this tissue, it has emerged the interest to evaluate and explore, for the first time, the role of α-adducin in the function and structure of the retina.

The main aim of the present work was to assess the effect of α-adducin in: a) the structure of the retina; b) the retinal function; c) the neuronal death of retinal cells.

This study was carried out using a KO-α-adducin mouse model (with the deletion of *Add1* gene). The retinal function was evaluated by electroretinography (ERG). The morphologic changes in the structure of the retina were observed by OCT and cresyl violet staining. The morphology of the retinal cells was addressed by immunofluorescence, whereas neuronal death by apoptosis was assessed using the terminal deoxynucleotidyl transferase dUTP nick end labeling (TUNEL) assay.

2. MATERIALS AND METHODS

2.1. Animals

C57BL/6 mice were obtained from the colony bred in the Institute for Research and Innovation in Health (i3S) animal house facility. The total population consisted of two groups: control (n=9) and KO-α-adducin animals (n=11) with deletion of *Add1* gene, accountable for the encode of α-subunit of adducin (α-adducin). Control and KO mice were obtained from heterozygous breeding pairs and genotyped by Institute for Molecular and Cell Biology (IBMC) CCGen facility, as described before in the literature (Robledo *et al.*, 2008).

Animals were maintained (2-3 animals in each cage) at 22 ± 1ºC on a 12h light/12h dark cycle, with fully access to water and food, and handled according with the Association for Research in Vision and Ophthalmology (ARVO) statement for the use of animals in vision and ophthalmic research.

2.2. Electroretinography

2.2.1. ERG recordings

Electroretinograms (ERGs) were recorded at postnatal day 100 (P100). After overnight dark adaptation period, the animals were anesthetized by intraperitoneal (IP) injection of 80/5 mg/kg ketamine/xylazine cocktail (ketamine: Imalgene 1000, Merial, Lyon, France; xylazine: Rompum®, Bayer, Leverkusen, Germany). Further, corneal anesthesia, with topical 4 mg/ml oxybuprocaine hydrochloride (Anestocil®, Laboratório Edol, Carnaxide, Portugal), and pupil dilation, with topical 10 mg/ml tropicamide (Tropicil®, Laboratório Edol), were carried out. During the procedure, hydroxypropyl methylcellulose (Methocel™ 2%, Dávi II – Farmacêutica S.A., Barcarena, Portugal) was used topically to keep the cornea hydration and a good electrical contact. The body temperature was maintained with a heating pad set to

37ºC. The electrical responses were recorded with the aid of three gold electrodes placed at the cornea, head (reference) and tail (ground).

The ERG waveforms were recorded with a bandwidth of 1 to 300 Hz and sampled at 3.4 kHz (except for flicker test, in which a 0.65 kHz sampling rate was used) by a digital acquisition system (Roland Consult GmbH, Brandenburg, Germany), and their analysis was carried out with RETIport software (Roland Consult GmbH, Brandenburg, Germany).

2.2.2. Light stimulation

Stimuli light was provided by a Ganzfeld stimulator (Roland Consult GmbH, Brandenburg, Germany). Four sequences were followed to obtain information about the functioning of retinal cell types (Rosolen *et al.*, 2008):

- Scotopic Luminance Responses: a series of white light flashes of seven different light intensities (0.0095 to 9.49 cd.s/m^2) were provided three times at 0.1 Hz to dark adapted animals;
- Photopic Adaptometry: white flashes with an intensity of 9.49 cd.s/m^2 were delivered three times at the onset of light adaptation and at 2,4,8 and 16 min with a frequency of 1.3 Hz, to light-adapt the animals;
- Photopic Luminance Responses: white flashes of seven different light intensities (0.0095 to 9.49 cd.s/m^2) were delivered three times at 1.3 Hz, with a white background light (25 cd/m^2), after 16 min of light adaptation. In this case, there was no retinal response for the lower light intensities.
- Photopic Flicker: white bright flashes (3.00 and 9.49 cd.s/m^2) were delivered ten times at 6.3 Hz, with a white background light (25 cd/m^2).

2.2.3. Data analysis of ERGs

The parameters obtained from the original ERG waveforms were:

- a-wave amplitude, measured from the graphical baseline to the a-wave dip;
- b-wave amplitude, measured from the a-wave dip to the b-wave peak;

- a-wave and b-wave latency (time to peak value), measured from the beginning of the stimulus to the a-wave trough and b-wave peak, respectively;
- individual OP amplitude and latency, measured as b-wave parameters after the application of a digital filter (Figure 2.1).

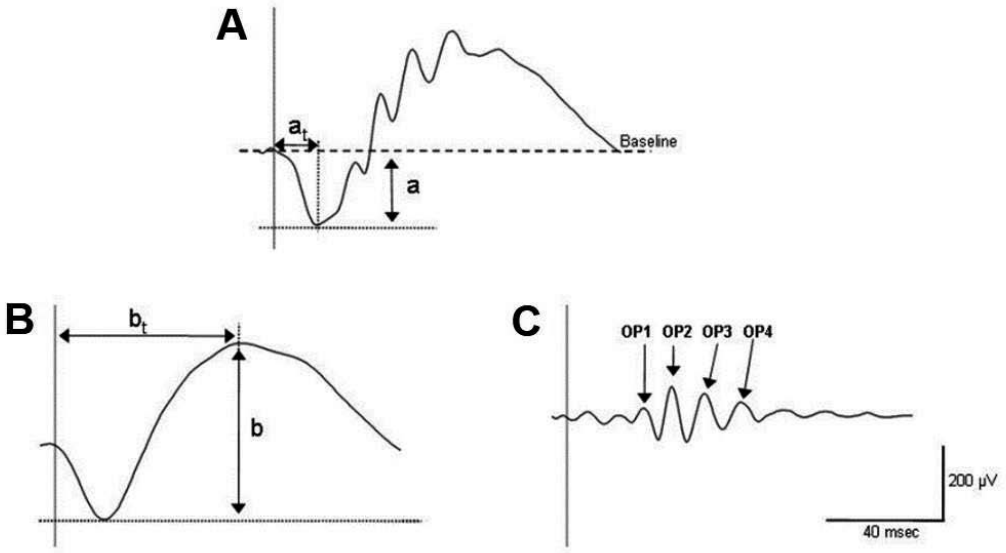

Figure 2.1. Typical ERG waveforms before and after digital filters application. **A**: original scotopic ERG waveform; **B**: isolation of b-wave from the original signal with a 50 Hz low frequency cut-off digital filter; **C**: isolation of individual OPs (OP1, OP2, OP3 and OP4) after application of 60 Hz high frequency cut-off digital filter. a – a-wave amplitude, a_t – a-wave latency, b – b-wave amplitude, b_t – b-wave latency (Adapted from Martins, J.,2014).

It is known that OPs and b-wave occur at different frequencies (Wachtmeister, 1998). Therefore, a digital low-pass filter with a cut-off frequency of 50 Hz was used to isolate b-wave from the original waveform (Zhang *et al.*, 2007). In contrast, to extract OPs from the original waveform, digital filters with a low frequency cut-off of 60 Hz for the scotopic ERG, and 55 Hz for the photopic ERG were used.

Using the fast Fourier transform (FFT), flicker responses were analysed. For statistical analysis, the amplitude and phase values for the fundamental, first (6.3 Hz) and second harmonics were obtained and considered.

In the statistical analysis, the parameters obtained for the right and left eye of each animal were averaged, once there was no significant difference between both eyes (see section 2.10).

2.3. Optical coherence tomography

To assess structural changes in the retina, *in vivo* Spectral Domain Optical Tomography (SD-OCT) (Phoenix Micron IV, Phoenix Research Labs, Pleasanton, CA) was performed. For that, the animals were anesthetized with an intraperitoneal injection of ketamine (80 mg/kg bodyweight) and xylazine (5 mg/kg bodyweight).

After corneal analgesia with topical oxybuprocaine and pupil dilation with topical tropicamide, fundus of the eye and tomographic images were collected from both eyes. In order to minimize animal pain once OCT technique involves the contact of a lens with the animal eye, we used ocular analgesia through topical oxybuprocain that does not affect the data provided by OCT. During all the technique, hydroxypropyl methylcellulose (Methocel™ 2%, Dávi II – Farmacêutica S.A., Barcarena, Portugal) was use topically to ensure cornea hydration and optical transparency.

The SD-OCT system used was able to capture 10 000–20 000 A scans per second with an axial resolution of 2 µm and a transverse resolution of 4 µm. For each eye, 13 tomographic images, obtained from line scans, plus the respective fundus of the eye, were acquired. The first image was acquired centered on the optic nerve head, followed by six scans above and six scans beneath that point. Thereby, globally, was evaluated a 1.700 µm high region in the retina (Alves *et al.*, 2018).

2.4. Tissue preparation for frozen retinal cross-sections

At P100, mice were deeply anesthetized with 80/5 mg/kg ketamine/xylazine and intracardially perfused with 0.1 M phosphate buffer saline (PBS) (137 mM NaCl, 2.7 mM KCl, 1.8 mM KH_2PO_4, 10 mM NaH_2PO_4, pH 7.4), followed by 4% paraformaldehyde (PFA) in 0.1 M PBS.

The eyes were enucleated, and fixed in 4% PFA in PBS, for 1 h, at room temperature. Then, the cornea was removed and the eyes were fixed in 4% PFA in

PBS, for 1 h, at room temperature. In a subsequent phase, the fixed eyes were transferred to 15% sucrose in PBS, overnight, at 4ºC, following 30% sucrose in PBS, overnight, at 4ºC. Finally, the eyes were embedded in a 1:1 30% sucrose and optimal cutting temperature compound (OCT compound) (Shandon™ Cryomatrix™, Thermo Fisher Scientific, Waltham, MA) solution. The samples were stored at -80ºC, until further use.

Retinal sections 10 µm- and 14 µm-thick were obtained on a cryostat (Leica CM3050S, Nussloch, Germany), at -20ºC, for cresyl violet staining and immunofluorescence/TUNEL techniques, respectively. Cryosections were collected on Thermo Scientific™ SuperFrost Plus slides, dried for 1h, at room temperature, and then stored at -20ºC, until further use. Ten slides (one slide having 10 µm-thick sections, and nine having 14 µm-thick) were prepared from each eye sample, each one containing eight eye slices (four from each eye).

2.5. Cresyl violet staining

Nissl substance is found in neurons, namely in the granular endoplasmic reticulum and ribosomes of soma and dendrites. By staining Nissl substance with cresyl violet, a global idea about the retinal histology is provided, once identifies the soma of neurons. However, this technique don't allow the observation of glial cells (Deitch and Murray, 1956; Humason, Gretchen L., 1962).

Cryosections 10 µm-thick were thaw for 10-20 min, at room temperature. The sections were fat free by defatting with xylene, for 10 min. After, dehydration was carried with ethanol following by a re-hydration sequence with 95%, 90%, 70% (v/v) ethanol for 2 min. The sections were then washed twice, in milliQ water, during 2 and 5 min, respectively. Further, sections were stained in 1% (w/v) cresyl violet (in miliQ water, C5042, Sigma-Aldrich Inc., St. Louis, MO) for 20 min and washed, in milliQ water, for 2 min. Subsequently, all sections were again dehydrated in ethanol (70%, 80%, 95% (v/v), 100%) and defatted twice in xylene, over 5 and 10 min (Wang *et al.*, 2010; Tsai *et al.*, 2014).

The sections were then cover slipped with DPX mounting medium (Sigma-Aldrich, Inc., St. Louis, MO). After drying, the coverslips edges were sealed with

clear nail polish, to prevent tissue sections from drying, and stored at 4ºC. Images were acquired using an upright microscope (Axio Lab. A1, ZEISS, Oberkochen, Germany) equipped with a CCD camera (Axio 105 Color, ZEISS) and the objectives A-Plan 5x/0.12 ∞/-, A-Plan 10x/0.25 ∞/-, A-Plan 40x/0.65 ∞/0.17 and the software Zen2 (blue edition) (ZEISS).

2.6. Immunofluorescence

14 µm-thick cryosections were thaw, for 10-20 min, at room temperature, and rehydrated twice, in washing buffer (PBS), for 5 min, to remove OCT and sucrose. The sections were surrounded with a hydrophobic barrier pen, in order to create a hydrophobic barrier and confine further incubation solutions.

Blocking and permeabilization were performed with 10% goat serum (Sigma-Aldrich, Inc., St. Louis, MO) and 0.5% Triton X-100 in PBS, in a humidified environment. Sections were then incubated overnight with primary antibodies (Table 2.1) diluted in 0.5% Triton X-100 in PBS, at 4ºC, in a humidified environment.

Table 2.1. Primary antibodies used in immunofluorescence.

Antibodies	Host	Working dilution	Supplier (catalog number)
Anti-Arrestin	Rabbit polyclonal	1:500	Merck Millipore, Burlington, MA (AB15282)
Anti-AP-2α	Mouse monoclonal	1:200	Santa Cruz Biotechnology, Inc., Dallas, TX (sc-12726)
Anti-Bassoon	Mouse monoclonal	1:2000	Enzo Life Sciences, Inc., Farmingdale, NY (ADI-VAM-PS003)
Anti-Brn3a	Mouse monoclonal	1:500	Merck Millipore, Burlington, MA (MAB1585)
Anti-Caspase 3	Mouse monoclonal	1:200	Santa Cruz Biotechnology, Inc., Dallas, TX (sc-7272)
Anti-GFAP	Chicken polyclonal	1:500	Merck Millipore , Burlington, MA (AB5541)

Anti-Calbindin D-28k	Rabbit monoclonal	1:500	Swant, Inc., Marly, Switzerland (CB-38a)
Anti-Iba1	Rabbit polyclonal	1:1000	Wako Chemicals, Inc, North Chesterfield, VA (019-19741)
Anti-OX6	Rat monoclonal	1:500	eBioscience, Inc, San Diego, CA (14-5321-82)
Anti PKC-α	Mouse polyclonal	1:500	Santa Cruz Biotechnology, Inc., Dallas, TX (sc-17769)
Anti-PSD95	Rabbit monoclonal	1:200	Cell Signalling Technology, Inc, Danvers, MA (3450)
Anti-Rhodopsin	Mouse monoclonal	1:500	Millipore, Burlington, MA (MABN15)
Anti-Vimentin	Rabbit monoclonal	1:500	Abcam, Inc, Cambridge, MA (ab92547)

Abbreviations: AP2-α, activating enhancer binding protein 2-α; Brn3a, brain-specific homeobox/POU domain protein 3A; GFAP, glial fibrillary acidic protein; Iba1, calcium-binding adapter molecule 1; OX6, MHC-II – major histocompatibility complex 2; PKC-α, protein kinase C-α; PSD95, postsynaptic density protein 95.

After washing with PBS (3×10 min), the sections were incubated with the corresponding secondary antibodies (Table 2.2) in 0.5% Triton X-100 solution in PBS, for 1h, at room temperature.

The negative control was made by incubating with the secondary antibodies only, in order to assess the fluorescence of these antibodies *per se*.

After washing with PBS (3×10 min), the sections were incubated with 1:5000 4’,6-diamidino-2-phenylindole (DAPI) in PBS. A final washing step with PBS was performed, 3×5 min (Fernández-Sánchez *et al.*, 2014).

Table 2.2. Secondary antibodies used in immunofluorescence.

Antibodies	Host	Working dilution	Supplier (catalog number)
Alexa Fluor® 568 Anti-Chicken IgG	Goat	1:500	Invitrogen, Thermo Fisher Scientific, Waltham, MA (A-11041)
Alexa Fluor® 488 Anti-Mouse IgG	Goat	1:500	Invitrogen, Thermo Fisher Scientific, Waltham, MA (A-11001)
Alexa Fluor® 488 Anti-Rabbit IgG	Goat	1:500	Invitrogen, Thermo Fisher Scientific, Waltham, MA (A-11008)
Alexa Fluor® 568 Anti-Rabbit IgG	Goat	1:500	Invitrogen, Thermo Fisher Scientific, Waltham, MA (A-11036)
Alexa Fluor® 568 Anti-Rat IgG	Goat	1:500	Invitrogen, Thermo Fisher Scientific, Waltham, MA (A-11077)

Abbreviations: IgC, immunoglobulin.

The sections were coverslipped using Glycergel Mounting Medium (Dako, Carpinteria, CA). After drying, the coverslips edges were sealed with clear nail polish, to prevent tissue sections from drying, and stored at 4ºC, in a dark slide box. Images were acquired using a fluorescence microscope, as detailed next (see section 2.8).

2.7. TUNEL assay

For the visualization of dying cells by apoptosis, TUNEL assay was performed, using a cell death detection kit (G3250, Promega, Madison, WI). This technique relies on broken deoxyribonucleic acid (DNA) strands generated during apoptosis, in an enzymatic reaction, via the labeling of free 3'-OH termini with modified nucleotides in an enzymatic reaction (Müller *et al.*, 2017).

The composition of solutions and buffers used in TUNEL assay is present in Table 2.3.

This procedure was performed at room temperature, unless otherwise stated. 14 µm-thick cryosections were thaw, for 10-20 min, and rehydrated twice, in PBS for 5 min, to remove OCT and sucrose. The sections were surrounded with a hydrophobic barrier pen, in order to create a hydrophobic barrier and confine further incubation solutions. Sections were incubated with 20 µg/ml proteinase K in proteinase K buffer, for 10 min, in order to permeabilize cells and facilitate the access to DNA for labeling in the following steps. After this incubation step, the sections were washed twice in PBS, for 5 min. As positive control, one section was pre-treated with DNase I buffer, for 5 min. It was followed by the incubation of 5.5 units/ml of DNase I in DNase I buffer, for 10 min, and washed twice. Positive control stained all nuclei in all layers of the retina (Müller *et al.*, 2017).

From this point onward, the steps involving positive control were performed independently, to avoid cross-reactions that could influence the results. The sections were equilibrated with equilibration buffer, for 10 min, and, then, incubated with recombinant terminal deoxynucleotidyl transferase (rTdT) incubation buffer containing nucleotide mix. This incubation step was performed, at 37ºC, for 60 min, in a humified chamber covered with aluminum foil to protect the sections from

sunlight. In the next step, the sections were placed in 2X saline-sodium citrate (SSC) (diluted from 20X SSC), for 15 min. The sections were washed with PBS (3×5 min) and, then, incubated with 1:5000 DAPI in PBS, for 10 min. Finally, the sections were washed with PBS, 3×5 min.

Table 2.3. Composition of buffers and solutions used in TUNEL assay.

Buffers and solutions	Composition
Proteinase K buffer	100 mM Tris-HCl (pH=8), 50mM EDTA
DNase I buffer	40 Mm Tris-HCl (pH=7.9), 10 mM NaCl, 6mM $MgCl_2$, 10 mM $CaCl_2$
Equilibration buffer	200 mM potassium cacodylate (pH=6.6 at 25ºC), 25 mM Tris-HCl (pH=6.6 at 25ºC), 0.2 Mm DTT, 0.25mg/ml BSA, 2.5 mM cobalt chloride
Nucleotide mix	50 µM fluorescein-12-dUTP, 100 µM dATP, 10 Mm Tris-HCl (pH=7.6), 1Mm EDTA
rTdT incubation buffer	90 µl equilibration buffer, 10 µl nucleotide mix, 2 µl rTdT enzyme
20X SSC	87.7 g NaCl, 44.1 g sodium citrate

Abbreviations: EDTA, ethylenediaminetetraacetic acid; DTT, dithiotretol; BSA, bovine serum albumin ; dUTP, deoxyuridine triphosphate, dATP, deoxyadenosine triphosphate; rTdT, recombinant terminal deoxynucleotidyl transferase SSC, saline sodium citrate

The sections were coverslipped using Glycergel Mounting Medium. After drying, the coverslips edges were sealed with clear nail polish, to prevent tissue sections from drying. Slides were stored in a dark slide box, at 4ºC, until images were acquired using a fluorescence microscope, as detailed next (see section 2.8).

2.8. Fluorescence image acquisition

Sections were observed with a fluorescence microscope (ZEISS, Oberkochen, Germany), using a LD Plan-Neofluar 40x/ 0.6 Korr Ph2 M27 objective and the software Zen2 (blue edition) (ZEISS). A certain number of images were taken, in order to scan all the retinal section, as is shown in Table 2.4. The groups were blind coded and captured under the same conditions.

Table 2.4. Number of images acquired to fluorescence image analysis, for both conditions.

Antibodies	Target Cell	WT	KO
AP2-α	(Displaced) Amacrine	99	223
Arrestin + Bassoon	Cones	5	28
Arrestin + Rhodopsin	Cones and Rods	126	172
Bassoon + PSD95	Synapses	157	254
Brn3a + PSD95	Ganglion	149	228
GFAP + Vimentin	Astrocytes and Müller	137	189
Iba1 + OX6	Microglia/macrophages	163	219
PKC-α + Arrestin	(Rod) Bipolar	11	51
PKC-α + PSD95	(Rod) Bipolar	162	279

2.9. Fluorescence image analysis

The approach followed for the quantitative and/or qualitative analysis of each immunolabelled retinal cell type was chosen accordingly. Images were analysed with *ImageJ* software (National Institutes of Health, Maryland, United States). When a quantitative analysis was performed, cells were counting as described below:

- Ganglion and amacrine cells: cells were manually counted. The ratio cells/total number of nuclei was calculated for each respective cell layer;
- Bipolar cells: the length of bipolar cells was manually measured;
- Cones: the region defined by the OS of cones was delimited by a segmented line which defined a closed area. The integrated density of that region was further determined;
- Microglial and activated microglial cells: a retinal length was defined by a segmented line, delimiting the region in which the cells were manually counted. The ratio cells/retinal length was calculated for each respective cell layer.

The images obtained for the labeling of Bassoon, PSD95, rhodopsin and PKC-α+Arrestin conjugation were just used for qualitative analysis.

Representative images were acquired with a laser scanning confocal microscope LSM 710 META (Zeiss, Oberkochen, Germany), using a C-Apochromat 40x/1.2 W Corr M27 and the software Zen2 (blue edition) (ZEISS).

2.10. Statistical analysis

The statistical analysis was based on an approach previously described (Campos, McVey and Astier, 2016), using SPSS version 20.0 (IBM Corp., 2011). The interquartile range (IQR, being IQR = Q3 – Q1) was used as the basis for identifying outliers. At the beginning, the extreme outliers were discarded based on the 3×IQR criterion which means the data points below Q1 – 3×IQR or above Q3 + 3×IQR were assumed as being too far from the central value to be acceptable. The Shapiro-Wilk test was, then, used to assess the normality of data (p>0.05) since samples (number of animals) were considered small (*i.e.,* n<50).

The normally distributed data were evaluated concerning the homogeneity of variance, using the Levene's test (p>0.05). An independent t-test was used to compare the means between only two groups for the same variable, WT and KO groups. The one-way analysis of variance (ANOVA) was used to determine whether there were significant overall differences (p<0.05) between the means of more than 2 (unrelated) groups. In this study, those groups were the retina of WT animals, and the retinas of KO animals with and without structural changes. To determine between which experimental groups differences would occur, the Fisher's Least Significant Difference (LSD) (p<0.05) was used. This is a *post hoc* test that is based on the smallest significant difference between two means, as if these means were the only to be compared, and not all the groups together (Williams and Abdi, 2010). Data were presented as mean $\pm$ standard error of the mean (SEM).

3.RESULTS

3.1. Effect of the deletion of α-adducin on retinal structure

For an overview of the eyes condition, photographs of the fundus of the eye were taken. In WT animals, the eyes exhibited a normal appearance (Figure 3.1.A), contrasting to what was observed in KO animals. Among all the photographs of KO mice, the lens opacity was consistent (Figure 3.1.C).

Furthermore, in order to assess retinal structure noninvasively, SD-OCT technique was performed. In this process, the incident low-coherence infrared light is split, travelling one part to the retina and the other to a reference mirror. Basically, the signal results from the interference pattern, subsequently processed into a signal, created by the interaction between the light coming back from the retina and the light reflected by the reference structure (Jaffe and Caprioli, 2004). As each retinal layer has different composition from the others, the absorption and reflection properties of the incident light are different, resulting in grey-scaled images (Hamdan *et al.*, 2012) that enable the easily identification of the retinal layers as can be seen in the tomogram of the eye of a WT animal (Figure 3.1.B). On the other side, when the same protocol was applied to the eyes of KO animals, and due to the lens opacity, a blurry image was obtained (Figure 3.1.D) which did not permit to observe the different retinal layers.

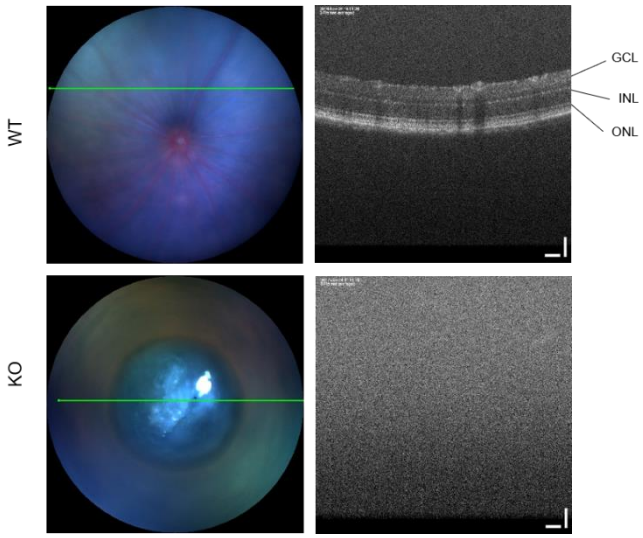

Figure 3.1. Legend on the next page.

Figure 3.1. Representative fundus image of the eye of a mouse showing the line scan (green line) (**A,C**) and the corresponding retinal tomographic images, revealing the spectral-domain OCT profile along the retina (**B,D**). Note the presence of lens opacity in the eye of a KO animal (**C**) which did not elicit the identification of the retinal layers **(D)** as can be seen in the eye of a WT animal (**B**). Scale bar represents 50 µm.

3.2. Effect of the deletion of α-adducin on scotopic ERG

3.2.1. Scotopic a-wave and b-wave

ERG technique was carried out to obtain information about neuronal and non-neuronal retinal cells function (Bayer *et al.*, 2001). In this technique, the electrical responses of these cells were obtained by stimulating the eye with light flashes varying in intensity, incrementally, from 0.0095 (-2 Log units) to 9.49 cd.s/m^2 (1 Log units). Despite the examination has been carried for other five intensities between -2 and 1 Log units, only the information regarding the two higher light flashes intensities was analysed since the amplitude of the electrical responses for the remaining ones was not high enough to assure a reliable analysis (Figure 3.2).

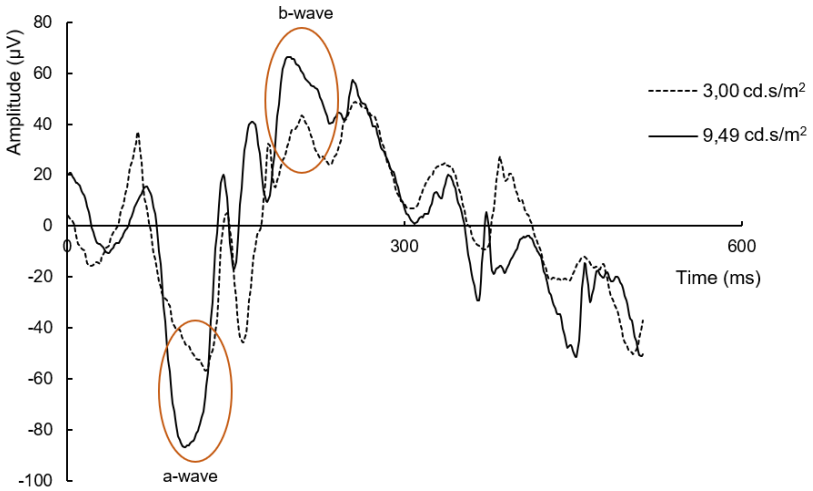

Figure 3.2. Representative recordings of scotopic ERGs in KO animals, achieved by the incidence of two different light intensities, 3.00 cd.s/m^2 (dashed line) and 9.49 cd.s/m^2 (solid line). Each trace represents an average of three responses to flash light stimuli of the same intensity. Increased flash ERG responses were obtained for the higher stimuli intensity; the same tendency was observed in the responses of WT animals. Solid vertical line indicates the onset of flash light stimuli.

In the two intensities presented in Figure 3.2, it was possible to clearly identify the a-wave and b-wave: the negative dip and the highest positive peak, respectively. As light flash intensity increased from 3.00 cd.s/m^2 to 9.49 cd.s/m^2, an increase in a-wave and b-wave amplitude in both conditions was also observed.

Comparing the profile of the recordings in KO and WT animals (Figure 3.3), it seems that a-wave and b-wave amplitudes in KO animals were lower than in WT animals.

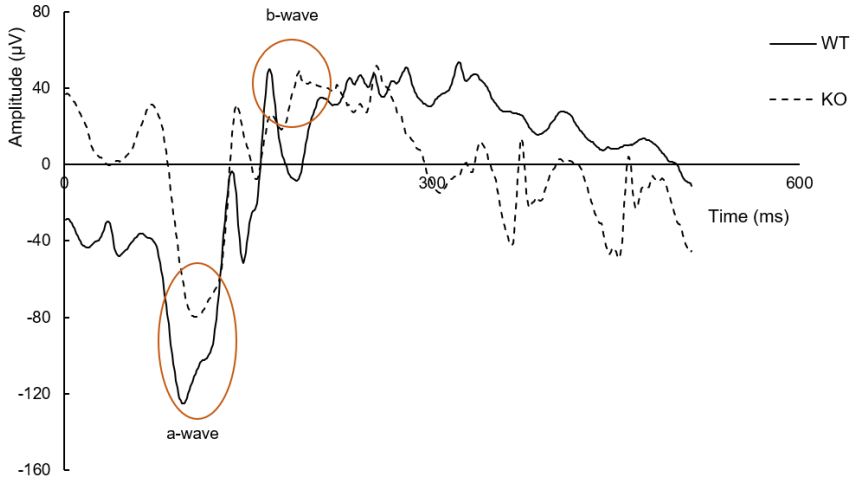

Figure 3.3. Representative recordings of scotopic ERGs in WT (solid line) and KO (dashed) animals, achieved by the incidence of 9.49 cd.s/m^2 light stimuli. Each trace represents an average of three responses to flash light stimuli of the same intensity. Reduced ERG responses and higher time to peak values were obtained in KO animals when compared to WT animals. Solid vertical line indicates the onset of flash light stimuli.

However, no statistical differences were found between WT and KO animals in both a-wave (Figure 3.4.A) and b-wave amplitudes (Figure 3.4.C). Regarding the latency time, values for a-wave and b-wave in KO animals were higher than in WT animals, being statistically significant only for the a-wave, for both intensities (p<0.05) (Figure 3.4.B).

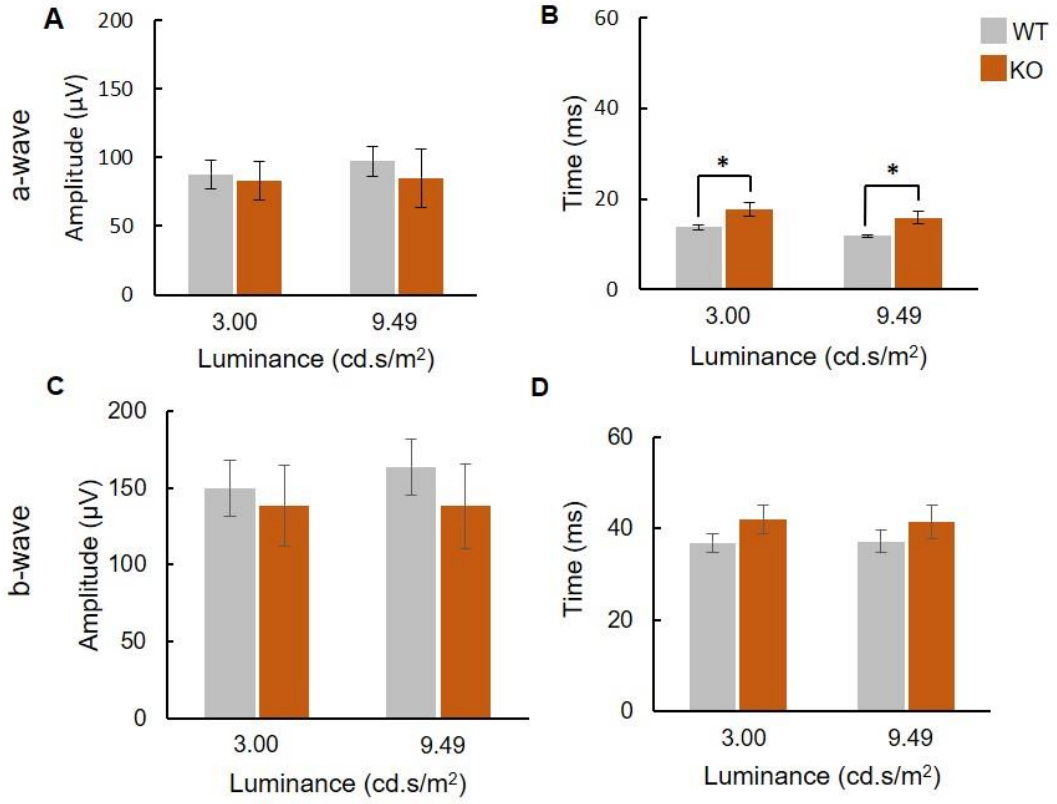

Figure 3.4. Effect of the deletion of α-adducin on a-wave and b-wave amplitudes (**A,C**) and latency times (**B,D**) in mouse scotopic ERG achieved by the incidence of 3.00 and 9.49 cd.s/m^2 stimuli. Regarding a-wave, for both intensities, KO animals had significantly augmented latency time values. Concerning b-wave, KO animals had decreased amplitudes and higher time to peak values, when compared to WT animals, although not statistically significative. Both parameters were analysed using t-test. Data are presented as mean±SEM (n=7-12). * p<0.05 - KO animals compared with WT animals.

To evaluate possible changes in b-wave amplitude conditioned by a-wave amplitude, the ratio between b-wave and a-wave amplitude (b-wave/a-wave ratio), was calculated for both luminances (Table 3.1).

Table 3.1. b-wave/a-wave ratio for both animal conditions. Parameter was analysed using t-test.

	WT		KO	
Lum (cd.s/m²)	**3.00**	**9.49**	**3.00**	**9,49**
Mean	1.821	1.715	1.744	1.518
SEM	0.194	0.110	0.244	0.149

Abbreviations: Lum, luminance.

The results showed that there were no statistically significant differences in b-wave/a-wave ratio, despite the slight decrease (5.0% and 11.5% reduction for 3.00 cd.s/m^2 and 9,49 cd.s/m^2, respectively) observed in KO animals when compared to the WT animals.

3.2.2. Scotopic oscillatory potentials

To evaluate the effect of α-adducin in synapses associated with inner retina, namely amacrine and ganglion cells (Wachtmeister, 1998), a digital filter with a cut-off frequency of 60Hz was applied in order to extract OPs components. It was possible to identify four OPs: OP1, OP2, OP3 and OP4. Concerning OPs amplitudes, for both intensities, a slight decrease was observed in KO animals (Figure 3.5.A-D), when compared to WT animals. Particularly in OP1 and OP2 amplitudes, it was observed a 20% and 37% decrease, respectively, for 9.49 cd.s/m^2).

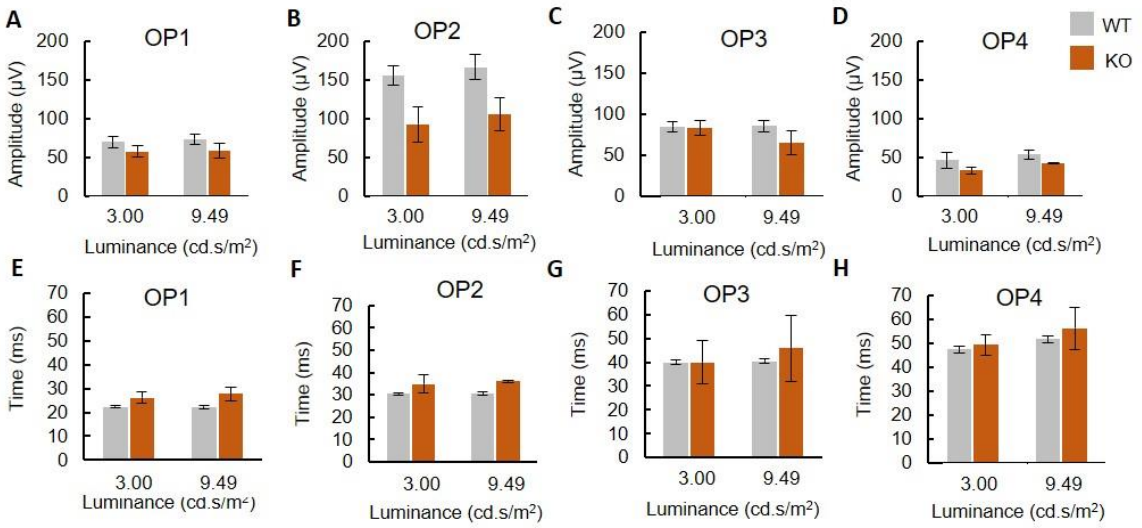

Figure 3.5. Legend on the next page.

Figure 3.5. Effect of the deletion of α-adducin on OPs amplitudes (**A-D**) and latency times (**E-H**) in mouse scotopic ERG achieved by the incidence of 3.00 and 9.49 cd.s/m^2 stimuli. Generally, KO animals presented lower amplitude and higher latency times in all OPs than WT animals. Both parameters were analysed using t-test. Data are presented as mean±SEM (n=7-12).

Regarding time to peak values (Figure 3.5.E-H), it seems that the delay between the delivery of the stimuli and the appearance of the respective OP for KO animals was higher than for WT animals, without statistically significance though. Particularly in OP1 and OP2 latency times, a 20% and 16% increase were observed, respectively.

It should be noticed that, in OP3 and OP4, values obtained in both amplitude and time to peak parameters were considerably disperse, with increased SEM values, possibly due to the conjugation of lower responses with the use of the filter that enabled the loss of information.

3.3. Effect of the deletion of α-adducin on photopic ERG

3.3.1. Photopic b-wave

For photopic ERG recordings, the animals were submitted to a light adaptation period, in which they were exposed to bright light flashes at the higher intensity (9.49 cd.s/m^2) at 2, 4, 8 and 16 min. After 16 min, the animals were completely light-adapted, and the respective ERGs were recorded (Figure 3.6). In this test, a-wave is not considered. Actually, since mice are nocturnal animals, they have a low density of cone photoreceptors (Melloni, 1971), the cells responsible for the photopic response.

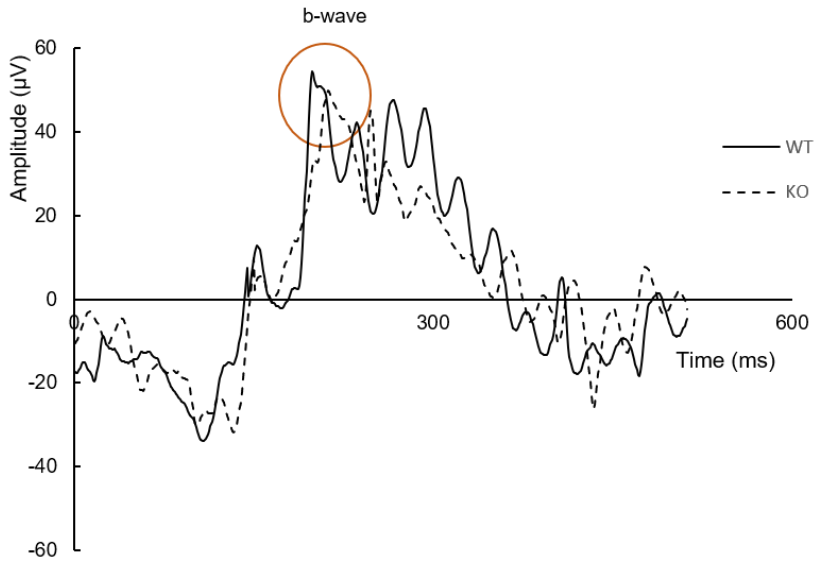

Figure 3.6. Representative recordings of photopic ERGs in WT (solid line) and KO (dashed line) animals, achieved by the incidence of 9.49 cd.s/m^2 stimuli, after 16 min light adaptation. Each trace represents an average of three responses to flash light stimuli of the same intensity. KO animal responses seemed to have slightly lower amplitudes and higher time to peak values comparatively to WT animal responses. Solid vertical line indicates the onset of flash light stimuli. Note that the vertical scale is different from Figure 3.3.

Using a similar procedure as in scotopic responses, a low-pass digital filter was applied, in order to extract b-wave components, that is, to remove higher frequencies from OPs. It was observed a tendency for lower amplitude (Figure 3.7.A) and higher latency time (Figure 3.7.B) in KO animals, comparatively to WT animals, in agreement with the representative recordings in Figure 3.6. These results are similarly to what was observed before in the scotopic response.

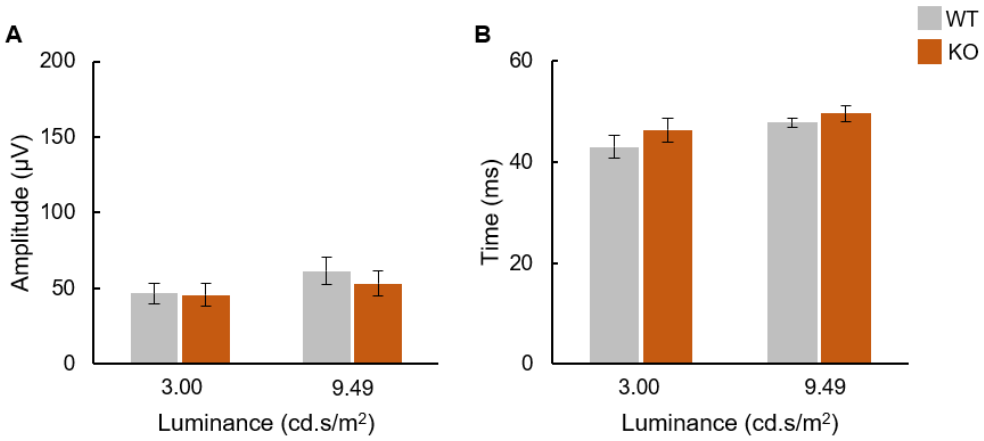

Figure 3.7. Legend on the next page.

Figure 3.7. Effect of the deletion of α-adducin on b-wave amplitude (**A**) and b-wave latency time (**B**) in mouse photopic ERG achieved by the incidence of 3.00 cd.s/m^2 and 9.49 cd.s/m^2 stimuli, after a light adaptation period. Responses of KO animals showed slightly lower amplitudes and higher time to peak values, comparatively to WT animals. Both parameters were analysed using t-test. Data are presented as mean±SEM (n=9-12).

However, no statistically significant differences were found between WT and KO animals, in amplitude and latency time, at both light intensities.

OPs signals could not be easily detected because of their small amplitude values. Therefore, OPs components were not extracted in the photopic response.

3.4. Effect of the deletion of α-adducin on photopic flicker ERG

In the photopic flicker ERG, responses are recorded in the presence of a rod-saturating background (Verma and Pianta, 2009). A pure cone response is, thus, obtained by stimulating the retina with high temporal frequency light stimuli (6.3 Hz), under light-adapted conditions (Figure 3.8).

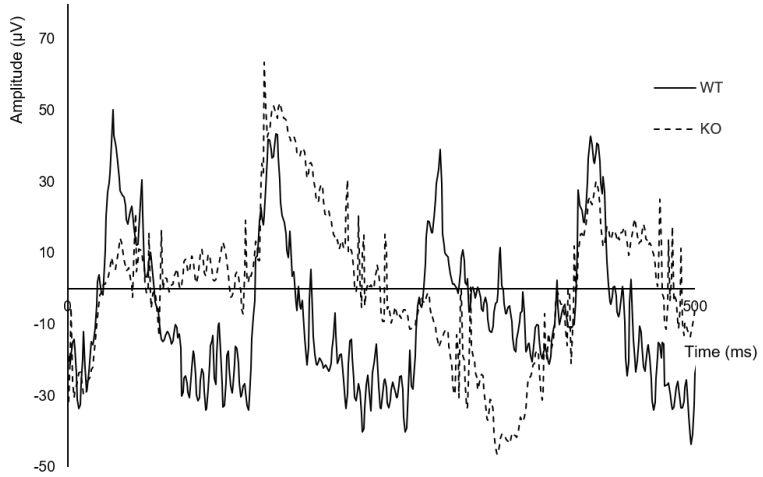

Figure 3.8. Representative recordings of photopic flicker ERGs in WT (solid line) and KO (dashed line) animals, for 9.49 cd.s/m^2, achieved at a frequency of 6.3 Hz using bright light flashes. KO animal responses seemed to have slightly lower amplitudes. Vertical line indicates the onset of flash light stimuli.

In the original traces, FFT was used to convert temporal into frequency domain to obtain the fundamental, first and second harmonic amplitudes and phase values, for the two higher intensities (3.00 and 9.49 cd.s/m^2).

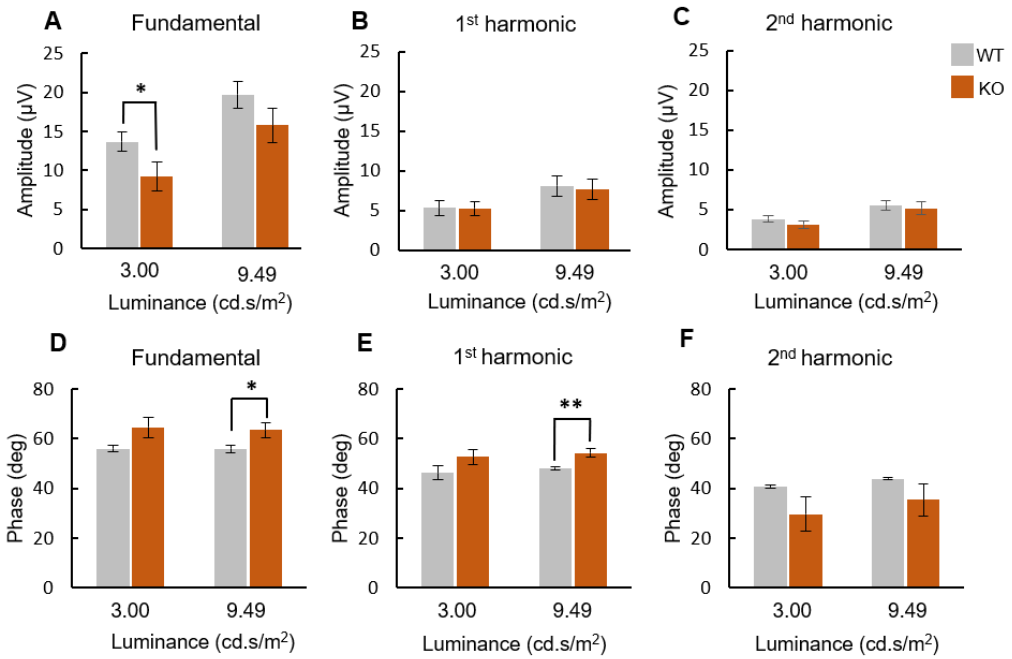

Figure 3.9. Effect of the deletion of α-adducin on pure cone response (flicker), namely on fundamental, first and second harmonic amplitudes (**A-C**) and phases (**D-F**). The photopic flicker responses were achieved at a frequency of 6.3 Hz using bright light flashes (light intensities of 3.00 cd.s/m^2 and 9.49 cd.s/m^2). There were consistent differences in fundamental wave amplitude between KO and WT animals, at 3.00 cd.s/m^2. In addition, fundamental wave and first harmonic phases had significantly augmented values in KO animals when compared to WT animals. Both parameters were analysed using t-test. Data are presented as mean ± SEM (n=9-12). * p<0.05, ** p<0.01 - KO animals compared with WT animals.

The results showed a decrease in fundamental wave amplitude in KO animals when compared to WT animals, being statistically significant only at 3.00 cd.s/m^2 (p<0.05) (Figure 3.9.A). Concerning first and second harmonic amplitudes, values are barely the same in both KO and WT animals (Figure 3.9.B,C). As for phase values, at the higher light intensity tested (9.49 cd.s/m^2), it was observed a statistically significant increase in KO animals, when compared to WT animals, regarding fundamental wave (p<0.05) (Figure 3.9.D) and first harmonic (p<0.01)

(Figure 3.9.E). In contrast with these results, a decrease in the second harmonic phase was found in KO animals, at both intensities, with no statistical significance though (Figure 3.9.F).

At the first, the presence of lens opacity in KO animals could difficult light rays to stimulate the retina and, consequently, hamper the acquisition of ERG recordings. However, the traces showed clear signals, meaning that the light intensity that reaches the retina, at the innermost layer of the eye, was enough to get a reliable and measurable electrical response.

3.5. Effect of the deletion of α-adducin on retinal histology

With OCT technique was possible to have an overview about the retinal layers in WT animals (Figure 3.1.B). To better understand the influence of this actin-capping protein in the retina, the histological stain was applied to identify the retinal cells and their phenotypes. Retinal cross-sections were stained with cresyl violet staining (Nissl substance). Here, the soma of the neurons is stained (Szalay *et al.*, 2016), allowing for the examination of the general retinal lamination, as well as to assess its integrity (Figure 3.10).

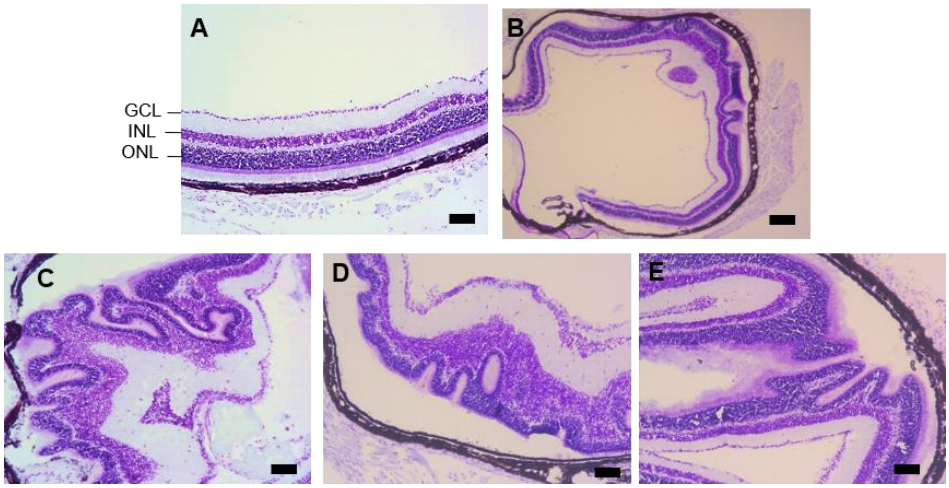

Figure 3.10. Representative images of retinal cross-sections stained with cresyl violet (Nissl substance) showing the retinal cell layers in WT (**A**) and KO (**B-E**) animals. Note the presence of an anomalous structure in KO animals retina, namely invaginations (**B**), vacuoles (**C**) and others (**D**). ONL seems to be the retinal cell layer more structurally affected. Histological images can be assigned to the cell layers that can be found in OCT images (*cf*.Figure 3.1.B). Scale bar represents 100 µm (**A,C,D,E**) and 200 µm (**B**) .

In WT animals, the retina presented a typical structure: the retinal cell layers were arranged uniformly and consistently (Figure 3.10.A), corroborating the results obtained by OCT. Conversely, in KO animals, the lack of α-adducin lead to striking structural changes in the retina (Figure 3.10.B), such as invaginations (Figure 3.10.C), vacuoles (Figure 3.10.D) and others (Figure 3.10.E). Accordingly, including thickening and narrowing of some cell layers was also observed. These data suggest that ONL, in which the cell bodies of photoreceptors are disposed, seems to be the most affected cell layer in consequence to the lack of this anti-capping protein.

Further, the length of the retinal cross-sections in WT and KO animals was determined in order to discard some influence of this parameter in the reliability of the subsequent results (Figure 3.11).

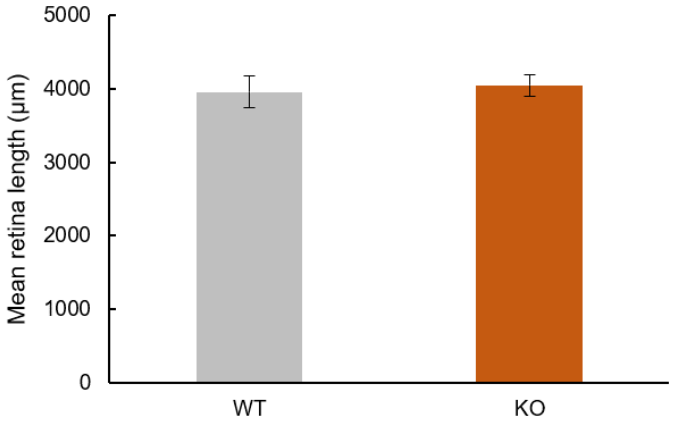

Figure 3.11. Comparison between the length of WT and KO retinal cross-sections obtained using Fiji software. No differences were observed in the retina length. Parameter was analysed using t-test. Data are presented as mean±SEM (n=9-12).

The length of the retinal cross-sections was similar between WT (4.00±2.22 mm) and KO (4.04±1.42 mm) animals.

The percentage of these atypical structures in the retina of KO animals was also important to be assessed. For that, the length of each retinal cross-section region displaying those structural changes was compared to the total retinal cross-section length. It was found that about of 25.6 + 6.09 % of the total retinal cross-section length in KO showed structural changes. Therefore, about three quarters of

the retina total extension in KO animals likely present a regular structure, similar to that in WT animals.

3.6. Effect of the deletion of α-adducin on retinal cells

Immunofluorescence was performed in order to better understand the effect of α-adducin on retinal cells. Here, each cell was labelled with a specific antibody, and then, this primary antibody was incubated with the respective secondary antibody coupled to a fluorophore. In this way, it was possible to identify the different cell types in all the layers and highlight the potential structural changes caused by the deletion of α-adducin.

The direction of light in the retina established the order of the following presentation of the results: from ganglion cells to photoreceptors. The information regarding microglial cells, astrocytes and Müller cells will also be presented.

3.6.1. Ganglion cells

Comprising 3% of the total retinal cells, RGCs are confined to the GCL and represent the final output of the retina (Zalis, Johansson and Englund-Johansson, 2017)**.**

Labelling Brn3a, a specific transcription factor highly expressed in RGCs innervating the principal retinothalamic/retinocollicular pathways (Quina, 2005), it was possible to detect the RGCs, presented in the GCL (Figure 3.12).

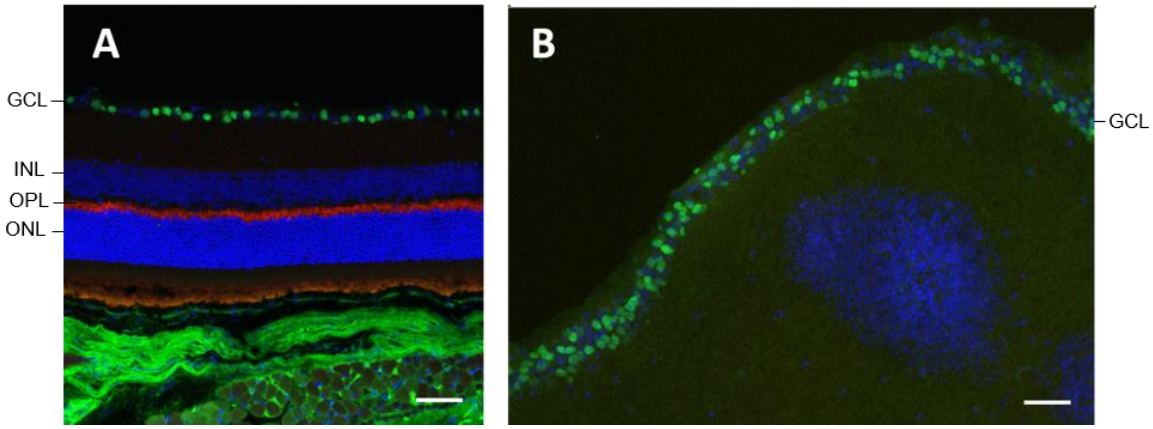

Figure 3.12. Legend on the next page.

Figure 3.12. Representative fluorescence photomicrographs of mouse retina cross-sections showing Brn3a (green) and PSD95 (red), and counterstained with DAPI (blue) from WT (**A**) and KO (**B**) animals. Scale bar represents 50 µm.

Immunofluorescence analysis of mouse retina revealed that, in WT animals, RGCs (Brn3a-positive cells) were disposed as a single layer (Figure 3.12.A). Conversely, in KO animals, Brn3a-positive cells were not so organized and displayed a random disposition (Figure 3.12.B).

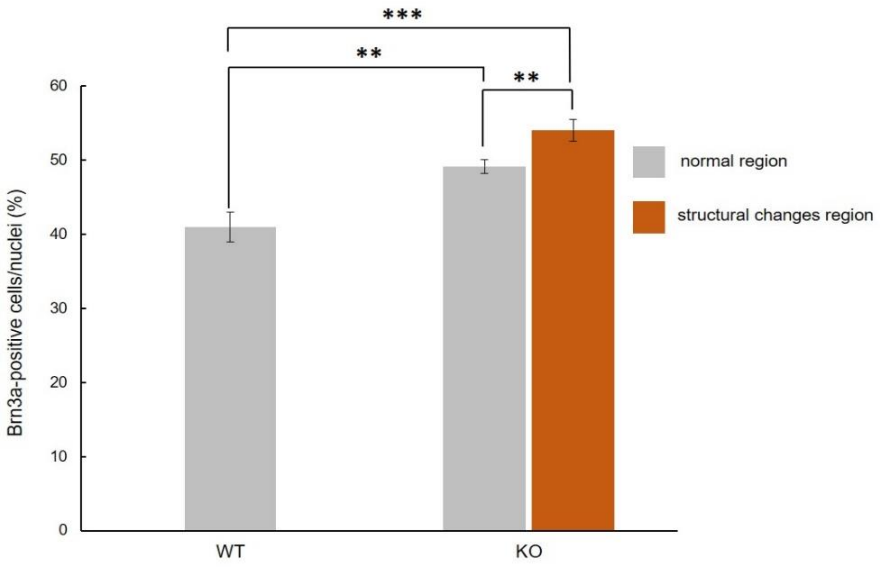

Figure 3.13. Brn3a-positive cells were expressed per number of total cell nuclei (%). KO animals had a significantly higher Brn3a-positive cells density when compared to WT animals, both in the retina regions where structural changes were and were not observed. Between the two distinct regions of KO animals there were also differences. Bars represent the mean±SEM for each condition (n=8). Statistical analysis was performed using t-test and ANOVA followed by the LSD test. ** $p<0.01$; *** $p<0.001$.

From the quantitative analysis, Figure 3.13 , it was found that Brn3a-positive cells density was statistically significantly higher in KO animals than in WT animals, both in the retina regions where structural changes were ($p<0.001$) and were not observed ($p<0.01$). Also, Brn3a-positive cells density was significantly higher in the regions containing structural changes comparing to the normal areas (similar to WT animals retina) of the retina ($p<0.01$).

It was also observed a 23% increase in the number of DAPI-positive cells (nuclei) in KO animals, at GCL, comparatively to WT. Once the ratio between Brn3a-positive cells/nuclei was the parameter used to evaluate RGCs (as described in section 2.9), an increase in the denominator (nuclei) will lead to a global decrease. Then, in KO animals, as was observed in the statistics (Figure 3.13), the increase of the number of Brn3a-positive cells needed to be higher to compensate it.

3.6.2. Amacrine cells

Being the most diverse class in the retina, amacrine cells are mainly found in the INL, where it has been estimated to make up 39% of the cells in this cell layer. However, amacrine cells can be disposed at GCL, as displaced amacrine cells (Lechner, O'Leary and Stitt, 2017) (Zalis, Johansson and Englund-Johansson, 2017).

By labelling the retinal cross-sections against AP-2α, an exclusive marker for amacrine cells, it was possible to distinctly observe the location of amacrine cells in both the INL and the GCL (displaced amacrine cells) (Figure 3.14) (Guduric-Fuchs et al., 2009).

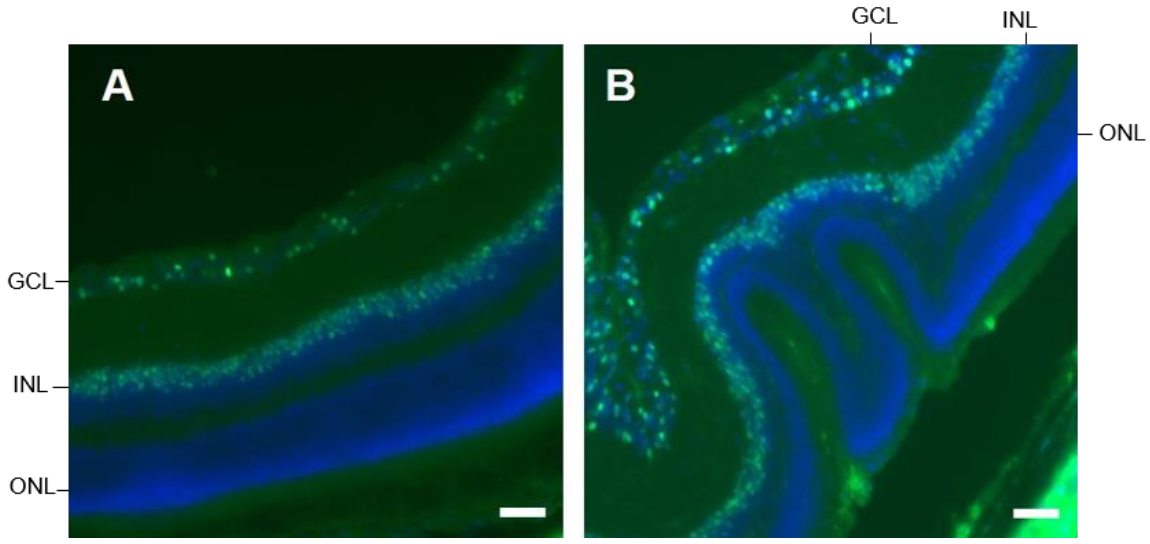

Figure 3.14. Representative fluorescence photomicrographs of mouse retina cross-sections showing AP2-α (green) counterstained with DAPI (blue) from WT (A) and KO (B) animals. Scale bar represents 100 µm.

From Figure 3.14, no differences seem to be detected between WT and KO mouse, with regard to amacrine cells density. So, in order to have a more reliable result, the number of amacrine cells in the GCL was quantified (Figure 3.15).

It is important to highlight that the quantification of amacrine cells in the INL was not carried out because there are diverse cell populations (such as amacrine, horizontal and bipolar cells) in this layer, which would hinder the visualization of focused amacrine cells in the plan of interest.

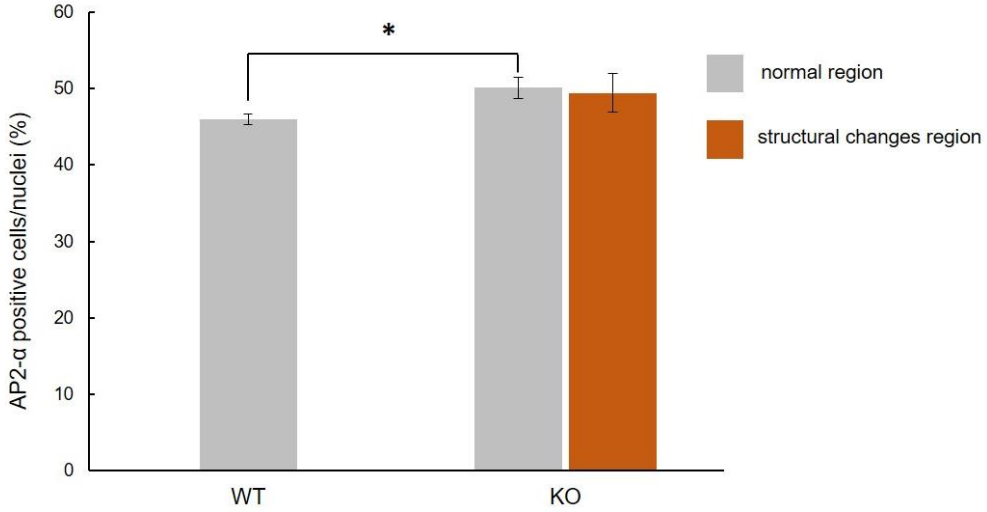

Figure 3.15. AP2-α-positive cells were expressed per number of total cell nuclei. Comparatively to WT animals, the number of AP2 - α-positive cells was significantly higher in KO animals, namely in the regions where structural changes were not observed. Bars represent the mean±SEM for each condition (n=8). Statistical analysis was performed using t-test and ANOVA followed by the LSD test. *p<0.05.

The quantitative analysis revealed that the number of displaced amacrine cells in the normal regions of KO animals was statistically significantly higher than in WT animals (p<0.05). Furthermore, in this situation, the number of displaced amacrine cells in the regions containing structural changes was similar to what was observed in the normal areas.

3.6.3. Bipolar cells

Bipolar cells, which represent about 41% of the cells in the INL, pass the visual signal from the photoreceptors to the inner retina, through synapses at the OPL and IPL level (Jeon, Strettoi and Masland, 1998). Despite span over a large extension, bipolar cells can be easily identified using a specific antibody such as PKC-α. Nevertheless, this marker is also expressed in a less extent by amacrine cells and cones (Zalis, Johansson and Englund-Johansson, 2017). PKC-α enabled the identification of the entire (rod) bipolar cell population once it is a molecular component of its signal transduction pathway regulated by calcium (Hernandez *et al.*, 2009).

The differences in the organization of (rod) bipolar cells were easily identified, as is demonstrated in Figure 3.16.

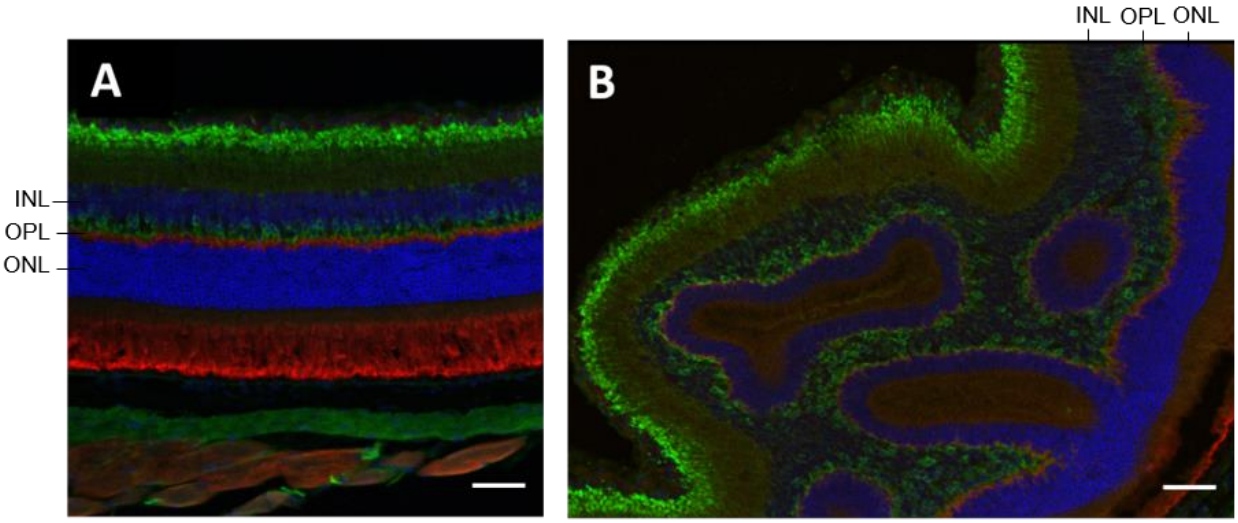

Figure 3.16. Representative fluorescence photomicrographs of mouse retina cross-sections showing PKC-α (green) and PSD95 (red), and counterstained with DAPI (blue) from WT (**A**) and KO (**B**) animals. Scale bar represents 50 µm.

In the retina of KO animals, bipolar cells presented different morphologies and orientations (Figure 3.16.B), and, overall, seemed to be disorganized. Besides, in the regions containing structural changes, it seemed that the length of bipolar

cells was affected, in contrast to the uniformity observed in the retina of WT animals (Figure 3.16.A).

Depending on the cell type, the analysis was made using parameters that characterized the cell and minimized the doubts in the quantification process. In the case of bipolar cells, once its quantification was extremely difficult, the chosen parameter was the length.

The statistical analysis (Figure 3.17) supported what was observed in the representative images obtained by immunofluorescence.

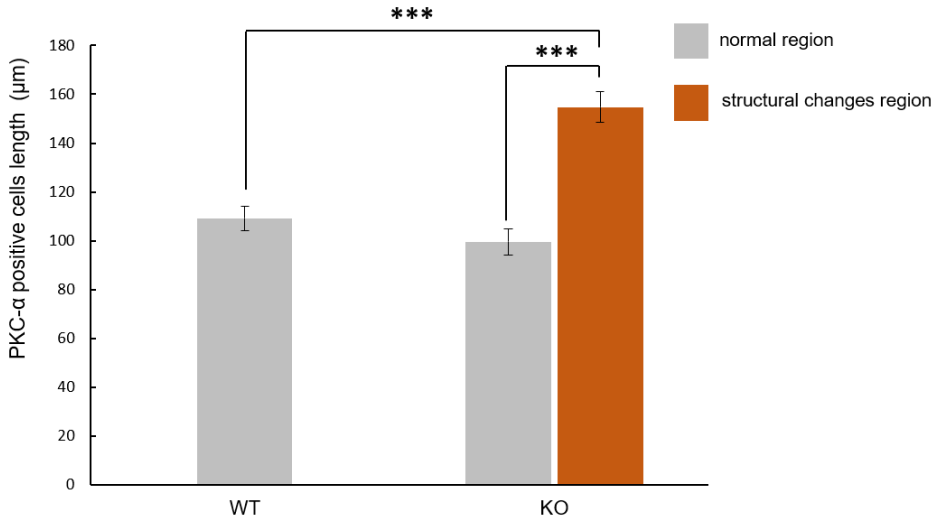

Figure 3.17. Bipolar cells were characterized by its length. The length of PKC-α positive cells was significantly higher in the retina regions of KO animals where structural changes were observed, comparatively to WT and to the normal regions. Bars represent the mean±SEM for each condition (n=4-5); Statistical analysis was performed using t-test and ANOVA followed by the LSD test. ****p*<0.001.

As can be seen in Figure 3.17, there was a statistically significant difference between the length of bipolar cells of WT animals and that of KO animals in the regions that contained structural changes ($p<0.001$). Moreover, in KO animals, the length of bipolar cells in the regions containing structural changes was significantly higher ($p<0.001$) than in the normal regions, meaning that somehow the presence of anomalous structures influences the organization and the span of these cells in the retina.

3.6.4. Horizontal cells

Being the less abundant cell population in INL (about 3% of all cells), horizontal cells establish synapses between photoreceptors and bipolar cells, at the OPL (Jeon, Strettoi and Masland, 1998).

Immunofluorescence analysis of horizontal cells was carried out using the molecular marker calbindin, a protein that binds Ca^{2+} with a high affinity, thus leading to prominent fluorescence in the cell body of horizontal cells (Wässle *et al.*, 1998) as can be observed in Figure 3.18.

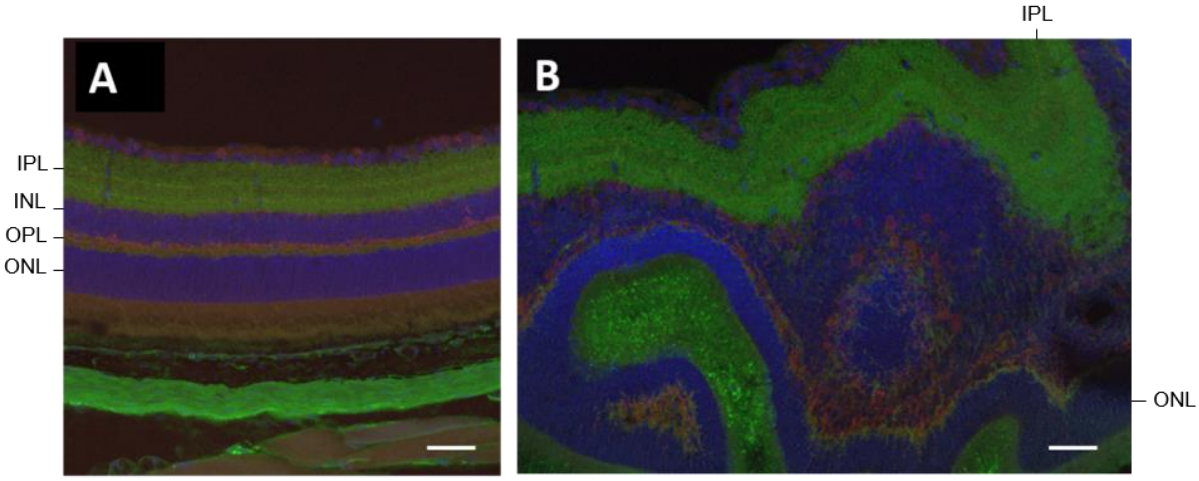

Figure 3.18. Representative fluorescence photomicrographs of mouse retina cross-sections showing calbindin (green) counterstained with DAPI (blue) from control (**A**) and α-adducin KO mouse (**B**). Scale bar represents 50 µm.

The results revealed that, in WT animals, horizontal cells were displaced in the OPL showing an organized pattern, as expected (Figure 3.18.A). On the other side, in KO animals, despite horizontal cells were also present in OPL, in some cases, their processes spanned to ONL. Also, it was notorious that these cells externally surrounded some structural changes (Figure 3.18.B).

Once the quantification of horizontal cells was extremely difficult, the statistical analysis was not performed.

3.6.5. Photoreceptors

Found in the outer part of the retina, photoreceptors comprise two types of cells: cones and rods, responsible for daylight and night vision, respectively (Kolb, Fernandez and Nelson, 1995).

Rhodopsin is a photopigment only present in the outer segments (OS) of rods whereas arrestin is part of a superfamily of regulatory proteins, only expressed in cone photoreceptors (Stöhr, Stojic and Weber, 2003; Coleman and Semple-Rowland, 2005). Thus, taking advantage of these two distinct and specific antibodies against them, rods and cones could be distinguished (Figure 3.19).

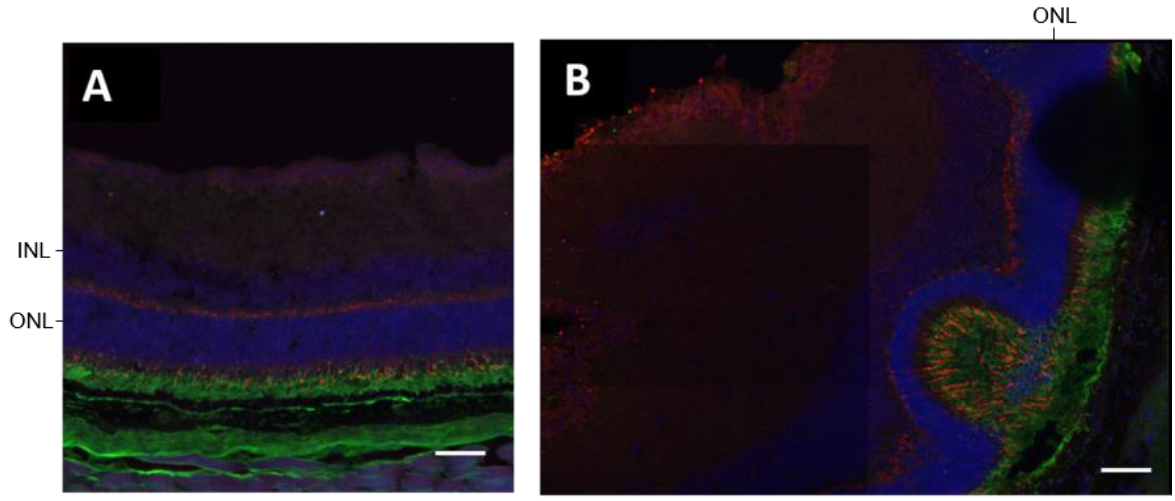

Figure 3.19. Representative fluorescence photomicrographs of mouse retina cross-sections showing arrestin (green) and rhodopsin (red), and counterstained with DAPI (blue) from control (**A**) and α-adducin KO mouse (**B**). Scale bar represents 50 µm.

As can be seen in Figure 3.19, WT and KO animals showed normal expression of arrestin in OS and synaptic terminals of cones. In addition, the retina of KO animals presented a non-uniform distribution of cone photoreceptors in contrast with the regular pattern seen in the retina of WT animals. Note that these cells adapted its orientation according to the shape and size of the anomalous structures typical in the retina of KO animals.

Concerning rods, due to its high density in the retina of nocturnal animals, they appeared as a uniform labelling which did not permit to observe their individual

arrangements. More importantly, these images showed that the outer layers where those in which the formation of anomalous structures, because of the deletion of α-adducin, was strongly evident.

Since the quantification of cone photoreceptors would not be feasible (due to higher number of these cells), it was decided to quantitatively analyse only cone photoreceptors through the integrated density in a region of interest, which is the product of the area defined by the operator and the mean grey value. Here, the delimited area of each image was defined by the outer segments of photoreceptors.

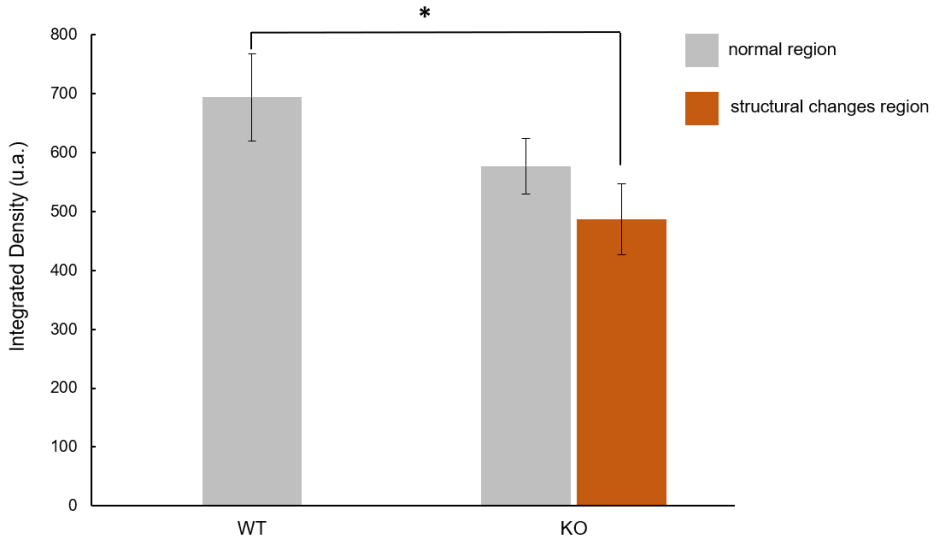

Figure 3.20. Cones were characterized by the integrated density. Overall, KO animals had a decreased density of cones, only with significance concerning the regions with the structural changes. Bars represent the mean±SEM for each condition (n=8). Statistical analysis was performed using t-test and ANOVA followed by the LSD test. *p<0.05.

From Figure 3.20, the results revealed a lower number/density of cone photoreceptors in KO animals than in WT animals. The difference was only statistical significative when WT animals were compared with the structural changes region of KO animals (p<0.05).

Furthermore, in KO animals, values obtained in the regions containing structural changes were lower than in the normal regions. Nevertheless, the differences were not statistically significant.

3.6.6. Microglia

Microglial cells are macrophages which are essential to maintain the homeostasis of CNS. In the retina, they can exist in two different states: in the dormant state (“surveying phenotype”), where the cells are principally found in the NFL, GCL and plexiform layers, and in the activated state (“alerted phenotype”) that can be induced by external stimuli or neural signals (such as inflammation) (Saijo and Glass, 2011).

The changes in microglial cells (Iba-1 positive cells) morphology were evaluated (Figure 3.21), since the deletion of α-adducin could have a role in inflammation.

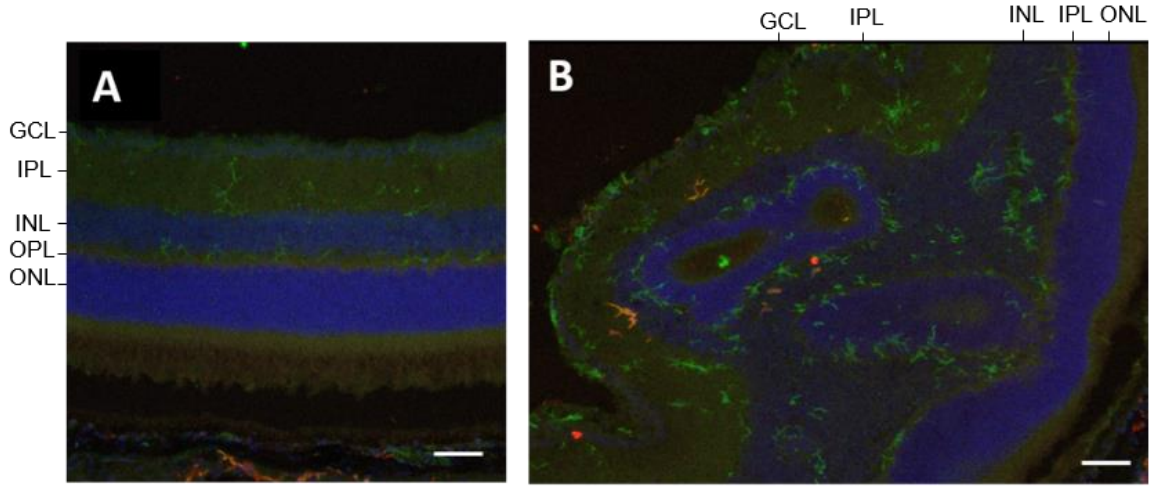

Figure 3.21. Representative fluorescence photomicrographs of mouse retina cross-sections showing Iba-1 (green) and OX-6 (red), and counterstained with DAPI (blue) from WT (**A**) and KO (**B**) animals. Scale bar represents 50 µm.

In Figure 3.21, by labelling microglial cells with Iba-1, an antibody specifically expressed in macrophages/microglia (Vecino *et al.*, 2016), it was possible to observe an increase in the number of Iba-1 positive cells in the retinal plexiform layers of KO animals comparatively to WT animals. Furthermore, in the retina of KO animals, some Iba-1 positive cells were observed in the retinal nuclear layers, but none of them had an activated phenotype.

As expected, OX-6, a determinant of the MHC class II present on activated/phagocytic microglia, was also detected in some microglial cells. It was

observed that OX-6 positive cells seemed to have an ameboid shape and a lower number of processes, comparatively to non-activated microglial cells.

The observed results are characteristic of an inflammatory condition (Karlstetter, Ebert and Langmann, 2010).

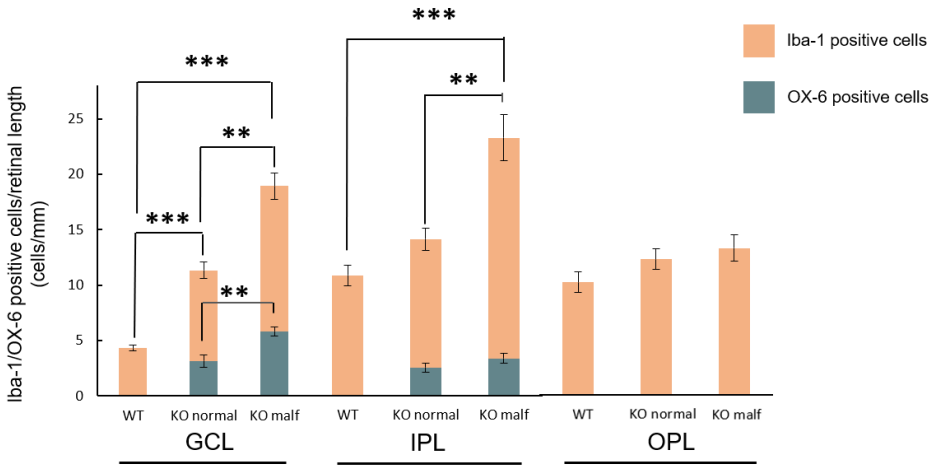

Figure 3.22. Iba-1 and OX-6 positive cells were expressed per retinal length (cells/mm). In GCL, KO animals had a significantly higher Iba-1 positive cells density when compared to WT animals, both in the retina regions where structural changes were and were not observed. In addition, the regions containing structural changes had a significantly higher OX-6 and Iba-1 positive cells comparatively to the normal regions. In IPL, there were also differences in the number of Iba-1 positive cells between the regions of KO animals that contained structural changes and WT animals and between the two distinct regions of KO animals. Bars represent the mean±SEM for each condition (n=3-8). Statistical analysis was performed using t-test and ANOVA followed by the LSD test. normal: region without structural changes; malf: region with structural changes. **p<0.01; ***p<0.001.

From the quantitative analysis (Figure 3.22), in the GCL, it was shown that the Iba-1 positive cells density was statistically significantly higher in KO animals than in WT animals, both in the retina regions where structural changes were (p<0.001) and were not observed (p<0.001). Further, Iba-1 positive cells density was statistically significantly higher in the regions containing structural changes than in the normal areas (similar to the retina of WT animals) (p<0.01). In the IPL, there was also observed a statistical difference between WT animals and the regions of KO animals that displayed structural changes (p<0.001) and between the two different regions of KO animals (p<0.01). In the OPL, the Iba-1 positive cells density

was slightly higher in KO animals than in WT animals, as same as between the regions containing structural changes and the normal areas, although with no statistical significance.

Regarding the OX-6 positive cells density, values obtained in the GCL and IPL of the regions containing structural changes were higher than in the normal areas of the retina of KO animals. These differences were statistically significant only in the GCL (p<0.01), though.

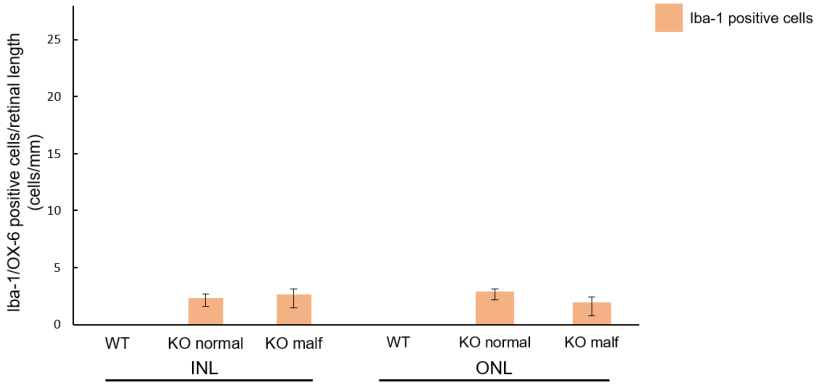

Figure 3.23. Iba-1 positive cells were expressed per retinal length (cells/mm). No statistical differences were found. Bars represent the mean±SEM for each condition (n=3-8). Statistical analysis was performed using t-test and ANOVA followed by the LSD test. malf: region with structural changes.

Finally, in the INL and ONL of KO animals, Iba-1 positive cells density was quite similar in both regions containing or not structural changes (Figure 3.23). In these layers, no OX-6 positive cells were detected.

3.6.7. Astrocytes and Müller cells

Astrocytes and Müller cells are macroglial cells located in the innermost part of the retina. Whereas GFAP, an intermediate filament protein, can be used to specifically identify astrocytes, Müller cells can be easily identified labelling vimentin, an intermediate filament-forming protein (Bringmann *et al.*, 2006).

As is shown in Figure 3.24, double immunolabelling allowed to clearly distinguish between these two types of cells.

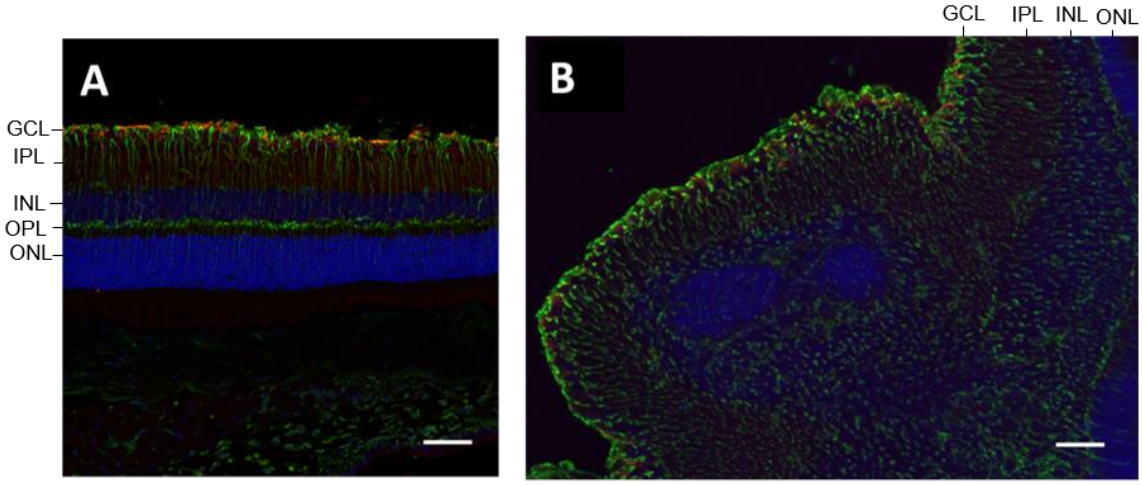

Figure 3.24. Representative fluorescence photomicrographs of mouse retina cross-sections showing vimentin (green) and GFAP (red), and counterstained with DAPI (blue) from WT (**A**) and KO (**B**) animals. Scale bar represents 50 µm.

Regarding astrocytes, a high fluorescence intensity seemed to be observed in the retina of KO animals, meaning likely the overexpression of GFAP in the NFL, which is a hallmark of retinal gliosis. The high intensity of GFAP was hampered by the high signalling of vimentin in the NFL, becoming more evident when the red-channel is observed alone.

Moving to Müller cells, they were disorderly disposed and achieved different depths in the retina of KO animals, contrasting to the uniformity observed in the retina of WT animals. Moreover, some Müller cells seems to express GFAP, which is also common in inflammation (Bringmann *et al.*, 2006).

3.7. Effect of the deletion of α-adducin on apoptosis

The TUNEL assay was carried out to ascertain if α-adducin deletion would impact on retinal cell death, by apoptosis (in a later stage) (Duan *et al.*, 2003). In TUNEL technique there is a recognition of DNA fragments generated by programmed cell death, called apoptosis (Weber and Langmann, 2013).

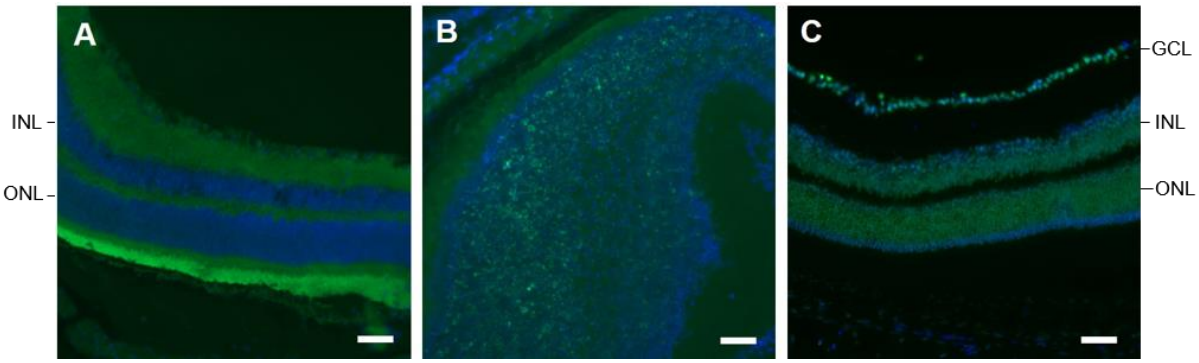

Figure 3.25. TUNEL assay on transversal frozen sections through P100 WT (**A**), KO (**B**) mouse retinas and in DNase-positive control (**C**). No apoptotic signal was detected except for positive control. Scale bar represents 100 µm.

Surprisingly, despite the structural changes described above typical in the retina of KO animals, no TUNEL positive nuclei were observed neither in KO nor in WT animals (Figure 3.25).

Once TUNEL assay is commonly used to detect apoptosis, in a later stage, we wanted to ensure that the cells were not dying via this process. For that, we labelled the retina cross-sections against caspase-3 (Figure 3.26), an early marker of apoptosis, aiming to identify apoptotic cells in tissue sections even before all the morphological changes of apoptosis occur (Tura *et al.*, 2009).

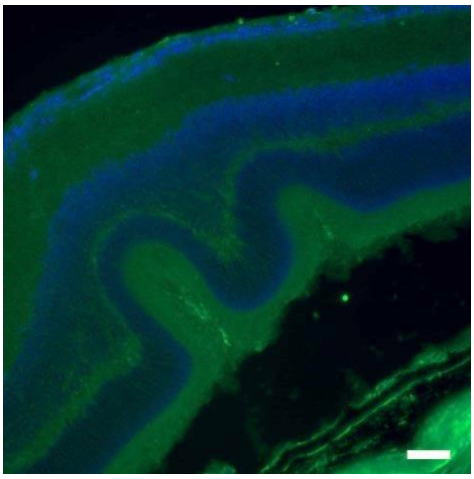

Figure 3.26. Representative fluorescence microphotograph of mouse retina-cross section showing caspase-3 (green) counterstained with DAPI (blue) from KO animals. Scale bar represents 100 µm.

Once more, as is shown in Figure 3.26, supporting the results obtained by TUNEL assays, the results showed no positive labelling in the retina of KO animals.

It is important to highlight that the label against caspase-3 was not carried out on the retinas of WT animals. We only stained the retina of one KO animal to rule out the cell death by apoptosis.

4. DISCUSSION

Adducins are a family of cytoskeleton proteins encoded by three closely related genes (α, β, and γ) whose activities are related to the stabilization of the neuronal cytoskeleton, namely on the bundling of actin filaments and on the recruitment of spectrin to these filaments (Gilligan et al., 1999; Matsuoka, Li and Bennett, 2000).

It is known that a disruption of the neuronal cytoskeleton may be an important trigger to neurodegeneration (Cairns, Lee and Trojanowski, 2004). Indeed, it was reported that adducins can regulate the activity of the actin cytoskeleton, destabilize synaptic contacts and lead to neuromotor impairment, contributing to cerebral palsy and ALS, in which elevated levels of phosphorylated adducin are detected (Kruer et al., 2013; Krieger et al., 2016). Adducin genetic variants (*ADD1,ADD2 and ADD3*) may also be relevant in schizophrenia pathology in humans due to alterations in synaptogenesis during the first stages of development (Bosia et al., 2016). Particularly, α-adducin can contribute to the regulation of endothelial barrier regulation. It was showed that α-adducin is involved in the remodelling of endothelial AJs (Kugelmann, Waschke and Radeva, 2015) and promotes the establishment of epithelial AJ and TJ, thus, controlling cell-cell contacts (Naydenov and Ivanov, 2011). It has also been shown that this adducin genetic variant directly impacts short and long-term memory, in nematode *Caenorhabditis elegans* (Vukojevic et al., 2012). In addition, methylation of the gene responsible for α-adducin in humans, *ADD1*, may contribute to hypertension (Bayoumy, El-shabrawi and Leheta, 2017).

Nevertheless, studies about the role of α-adducin on the ocular system are very scarce. Only one focused on the influence of α-adducin in the maintenance of axon diameter, demonstrated the role of this gene in the retina, particularly in the optic nerve (Leite et al., 2016).

Given that it was shown that the deletion of α-adducin lead to axon enlargement and subsequent degeneration of the optic nerve (Leite et al., 2016), we were challenged to investigate the role of α-adducin on retinal physiology and

structure. To the best of our knowledge, this is the first study showing the role of an adducin protein on the structure and function of the retina.

In this project, the α-adducin KO mice was used as study object. The analysis of their nervous tissue revealed that the levels of β- and γ-adducin were severely decreased (Leite *et al.*, 2016). In addition, no adducin complex formation was verified in the absence of the α-subunit, the limiting subunit in tetramer formation. As the stability of the other isoforms is severely affected, the α-adducin KO mice can be seen as a complete KO for adducin (Robledo et al., 2008, 2012).

The effect of α-adducin deletion on the retinal structure was evaluated by OCT. This is a non-invasive technique commonly used in clinical practice, which allows for the observation of changes in the thickness of retinal cell layers, as consequence of ocular diseases, such as diabetic retinopathy (Sanchez-Tocino *et al.*, 2002).

The images of the fundus of the eye revealed the opacity of the lens of KO animals (Figure 3.1.C) that disabled the visualization of the retinal cell layers as it was performed in WT animals (Figure 3.1.B). We hypothesize that the deletion of α-adducin enabled the deposition of substances in the lens, such as proteins, cholesterol and phospholipids (Huang and Chen, 2018). Despite it was not possible to observe the retinal cell layer pattern in KO animals (Figure 3.1.D), we can speculate that alterations in the retinal thickness of the ONL were likely to occur, since the clearest and most prominent morphological changes were seen further in the outer retina by histological staining (Figure 3.10.B-E).

In order to understand the role of α-adducin on retinal physiology, we performed ERG. This is a non-invasive technique also used in clinical practice aiming to detect alterations in the retinal physiology that are related with some eye diseases (Rosolen *et al.*, 2008).

Under dark-adapted conditions, there was a tendency for a lower amplitude of a-wave, the first negative peak of scotopic ERG, in KO animals, comparatively to WT animals (Figure 3.4.A). The time to peak values of the a-wave were significantly higher in KO animals, compared to WT animals, for both higher intensities (Figure 3.4.B). These results suggested that, in the absence of α-adducin, photoreceptors (mainly rods) take longer to respond to the light stimuli but their function is only mildly hampered.

Concerning Müller and ON bipolar cells (responsible for b-wave in scotopic response), in the inner layers, we observed a tendency for a lower amplitude and higher latency time of b-wave in the KO animals relatively to the WT animals (Figure 3.4.C,D). The tendency observed in b-wave amplitude is likely to reside in the a-wave generating mechanism, induced by photoreceptors, since no significant differences were detected in b-wave/a-wave ratio in both KO and WT animals, for 3.00 cd.s^2 and 9.49 cd.s^2 intensities (Table 3.1).

Regarding oscillatory potentials, the same tendency was observed: a lower amplitude and higher time to peak values in KO animals compared to WT animals which suggest that synaptic activity, involving amacrine and ganglion cells, in the inner retina, was slightly impaired (Figure 3.5). These results are similar to those already described in some eye diseases, such as diabetic retinopathy, in which OPs parameters were significantly reduced (Holopigian *et al.*, 1992; Wachtmeister, 1998).

The photopic responses revealed a tendency for a lower amplitude and a higher latency of b-wave in KO animals, when compared to WT animals (Figure 3.7). As in high light intensities b-wave results from the activity of ON and OFF bipolar cells (Stockton and Slaughter, 1989), the results suggested a slightly impairment of their function. Summarizing, the results of b-wave for scotopic and photopic responses pointed slightly alterations in the function of Müller and bipolar cells.

In the flicker test, rods are saturated and a pure cone response is obtained (Verma and Pianta, 2009). Our results show that the fundamental wave amplitude was significantly lower in KO animals for 3.00 cd.s^2 (Figure 3.9.A) On the other side, the implicit times of fundamental wave and first harmonic were significantly increased in KO animals, compared to WT animals for 9.49 cd.s^2 (Figure 3.9.D,E).

Thus, it can be concluded that, in line with the results obtained from the scotopic a-wave (mainly generated by rods), cones function was significantly impaired. We believe that this may be related to the decrease in the integrated density of cones in KO animals (Figure 3.20) further observed by immunofluorescence (Figure 3.19), i.e., less cones are likely to entail less electrical signal.

In the literature, it has been reported that cataracts impact on ERGs recordings. As the cataract grade increases, the amplitude and the implicit time of the flicker ERG components lowers and increases, respectively (Miura *et al.*, 2016). Thus, we cannot exclude that the opacity in the lens of KO animals may have affected the ERG recordings. However, the results showed that the light intensity that reached the retina was enough to stimulate the retinal cells and to give rise to the ERG electrical signals.

Despite the retinal function be only mildly impaired in the absence of α-adducin, the structural changes were clearer and more evident. Histological images of the retina of KO animals revealed the presence of various structural changes in about 26% of its extension (Figure 3.10.B-E), that was not influenced by the length of the retina (Figure 3.11). Therefore, despite the presence of these anomalous structures, the remaining three quarters of the retina with regular structural organization seemed to be enough to ensure retinal function, as demonstrated in ERG recordings.

The iBRB and the oBRB are composed, among others, by endothelium and epithelium (RPE), respectively (Pournaras *et al.*, 2008). Also, the presence of TJ in the two barriers, which are in continuous remodulation, regulates the flow of fluids and molecules between blood and retina. Thus, a disruption of the TJ arrangement can lead to the accumulation of these substances in the retinal space (Cunha-Vaz, 2009). It was reported that adducins have a direct role in the regulation of actin dynamics, which is critical for endothelial and epithelial function (Naydenov and Ivanov, 2011; Kugelmann, Waschke and Radeva, 2015).

Recently, it was found that the activation of microglia led to the disruption of BRB, causing the accumulation of sub-retinal fluid in the retinal space. Therefore, the structural alterations can also be related to the inflammation mediated by microglia cells (Kokona, Ebneter and Zinkernagel, 2017).

Several reports have shown that the expression of Iba-1 is upregulated in microglia following by injury, for example, due to nerve axotomy (Ito *et al.*, 1998), ischemia (Ito *et al.*, 2001) and several brain diseases (Eitzen *et al.*, 1998). In the retina, the deletion of α-adducin seems to induce the increase of Iba-1 positive cells, as well as their activation, in the GCL and the IPL, particularly, in the regions of the retina where structural changes were observed (Figure 3.22). This is in agreement

with previous reports showing that microglial cells migrate to the site of injury (Hanisch, 2002).

The distribution of Iba-1 positive cells in the retina of KO animals seems also to be altered. Whereas, in WT animals, Iba-1 positive cells were mainly present in the GCL and plexiform layers (Figure 3.21.A), in KO animals, these cells spanned to the nuclear layers and sometimes their processes crossed all the thickness of the layer (Figure 3.21.B). This is known to be a common feature of neuroinflammation condition, as already reviewed (Madeira *et al.*, 2015). Interestingly, in KO animals, we detected some Iba-1 positive cells in the ONL (Figure 3.23), where the cell bodies of photoreceptors are located. Recently, it was showed that microglia activation can initiate or accelerate photoreceptor degeneration (Blank *et al.*, 2018). This may also explain the apparent decrease of the number of (rod) photoreceptors as consequence of the deletion of α-adducin.

Moreover, the higher increase in the number of Iba-1 and MHC-II positive cells was detected in the IPL and GCL (Figure 3.22), the last where has been proved that the number of ganglion and displaced amacrine cells was significantly increased, when comparing KO and WT condition (Figure 3.13 and Figure 3.15). We expected that, if the inflammation process was responsible for the observed alterations, the number of ganglion cells would decrease (Sivakumar *et al.*, 2011), however there should be some mechanism, for example a neurodevelopmental alteration, that might explain this unexpected observation.

The inflammatory process was also characterized by the changes in the reactivity of other macroglial cells. We observed that the levels of GFAP and vimentin seemed to be up-regulated in astrocytes and Müller cells, as usual in a gliosis condition (Figure 3.24). In addition, in the retina of KO animals, we observed that some Müller cells also express GFAP, a marker only present in astrocytes, under normal conditions (Coorey *et al.*, 2012; Fernández-Sánchez *et al.*, 2015). Accordingly with the literature, high expression levels of GFAP in Müller cells have been associated to different types of ocular damages, including glaucoma, diabetic retinopathy, and retinitis pigmentosa (Strettoi *et al.*, 2002; Wang *et al.*, 2002; Gerhardinger *et al.*, 2005).

We hypothesized that structural (and likely others) changes observed in some cell types can be influenced by other cell types. Our results showed alterations in the structure and number of horizontal (Figure 3.18) and amacrine cells (Figure 3.15), respectively, which means that lack of α-adducin affected these cells. For example, it was shown that in a coneless mouse, the terminal branching pattern of horizontal cell dendrites is altered (Reese, 2005).

Our results might indicate that each cell type change its morphology accordantly to the environment and to the neighboring cells, during the retinal development. For instance, in KO animals, the stretching observed in some axons of bipolar cells (Figure 3.16.B and Figure 3.17), the last neuronal cell type in the retina to be differentiated , suggests that these retinal cells have elastic properties and are able to adapt its morphology, in order to maintain its function as a transmitter of information between photoreceptors and ganglion cells (Cepko, 2014; Euler *et al.*, 2014). The appearance of b-wave in scotopic (Figure 3.3) and photopic (Figure 3.6) responses corroborates this statement since bipolar cells are involved in its generation mechanism (Miller and Dowling, 1970; Stockton and Slaughter, 1989).

It was reported that deletion of α-adducin leads to axonal enlargement and consequent degeneration in the optic nerve (Leite *et al.*, 2016). Since the optic nerve is the bundling of ganglion cells axons, we would expect that the number of ganglion cells would be diminished in KO animals, as already mentioned. Surprisingly, we observed a significant increase in the ratio between Brn3a-positive cells and the number of nuclei in the GCL of KO animals (Figure 3.13). We further counted the number of DAPI-positive cells (nuclei) and we concluded that values in KO animals were higher than in WT animals. Further studies are needed to fully clarify this issue.

In most results, the effect of the deletion of α-adducin was more exacerbated in retinal regions of KO animals in which structural changes occurred. However, there were also statistical differences in the quantification of the cells between WT and the normal areas of KO animals, which means that the influence of α-adducin did not exclusively affect the area involving the malformations but instead affected other retinal regions.

Finally, we assessed the effect of the deletion of α-adducin on cell death by apoptosis. We did not observe any evidence of cell death neither by TUNEL assay nor by active caspase-3 labelling (Figure 3.25 and Figure 3.26), so cells are not

dying by apoptosis. Again, this seems to be not in agreement with some of our results, namely, the apparent reduction in the number of photoreceptors in KO animals. However, since activated microglial cells were detected, cytokines like TNF-α are likely to be released and, possibly, inducing cell death via other mechanism (Hanisch, 2002). Other cell death mechanisms, like necrosis, are also to be considered.

Overall, this study showed that analyzing the retina can be a useful approach to investigate CNS diseases since the eye is the only part of the CNS that can be investigated non-invasively, sharing many characteristics with the brain (MacGillivray et al., 2014). So, we may hypothesize that α-adducin also induces changes in the brain development, organization and function, but evidences to confirm this hypothesis are still lacking.

5. CONCLUSIONS AND FUTURE DIRECTIONS

We detected several differences in the eye and the retina of KO-α-adducin mice, at P100, comparing with age-matched WT mice. The deletion of α-adducin induced opacity of the lens that did not enable the *in vivo* visualization of the retinal layers.

By electroretinography, regarding scotopic a-wave, we found that the time response of photoreceptors was significantly increased. Moreover, by histological staining, it was detected the presence of structural malformations in about 26% of the retinal extension. Using antibodies specific for retinal cell types, we found an apparent worsening of the organization of cones, amacrine and horizontal cells and a higher density of ganglion and amacrine cells. Moreover, there was a significant increase in the length of bipolar cells and an abnormal morphology of these cells was also detected. These characteristics were associated with an inflammatory situation, as was demonstrated by the abnormal density, reactivity and distribution of microglial cells, namely in the GCL and IPL. The reactivity of astrocytes and Müller cells seemed also to be increased. Nevertheless, no cell death by apoptosis was detected.

Summarizing, the deletion of α-adducin does not cause significant effects in retinal physiology, since most of the parameters of ERG recordings were not altered, but impacts massively on the retinal structure, changing the morphology, distribution and reactivity of specific retinal cell types.

We showed, for the first time, that the deletion of α-adducin lead to structural changes in the retina. The structural alterations could be (i) directly induced from the deletion of the protein, (ii) partly mediated by the inflammatory process driven by microglial cells, (iii) influenced by other unknown mechanisms. With this work it was not possible to clarify these points, which justifies further studies. Other immunofluorescence markers should be used to elucidate the origin of the structural changes, namely via the identification of aquaporins and TJ junction components, like claudins, in the BRBs.

Most of the features observed in the retina of α-adducin-KO mice, like inflammation, have also been reported in the brain, under CNS neurodegenerative diseases (Vukojevic *et al.*, 2012; Bosia *et al.*, 2016; Krieger *et al.*, 2016). Therefore, we believe that the retina may act as window to screen some of these diseases. However, further studies are needed to clarify it.

Despite the results here described, further studies are needed in order to better understand the effect of adducin family on the CNS, bother retina and brain. These studies should be performed at earlier time points (even in embryonic phases) according to the retinal development, to investigate when and how this protein starts to impact the retina. This approach will also be important to conclude if the microglial cells have an influence on the retinal structural alterations. Are the structural alterations the effect of the inflammation caused by the lack of α-adducin? Or, the inflammation, mediated by microglial cells, does not impact on the structure of the retina, affecting only its cells? The quantification of pro-inflammatory markers, such as TNF-α and interleukins, is also important to assess.

In this work, some of the results were intriguing. The increased number of ganglion and amacrine cells should be clarified. For instance, it would be interesting to measure the diameter of the axons in the optic nerve to fully characterize the RGCs.

The use of retinal whole-mounts will also be important to avoid the loss of information that can occur when working with cross-sections.

Since the lack of α-adducin is involved in the regulation of synaptic strength, in the future, we expect to clarify this issue.

6. BIBLIOGRAPHY

Alves, M. R. P. *et al.* (2018) 'Subtle thinning of retinal layers without overt vascular and inflammatory alterations in a rat model of prediabetes.', *Molecular vision*, 24, pp. 353–366.

Bayer, A. U. *et al.* (2001) 'Evaluation of different recording parameters to establish a standard for flash electroretinography in rodents', *Vision Research*, 41(17), pp. 2173–2185.

Bayoumy, N. M. K., El-shabrawi, M. M. and Leheta, O. F. (2017) 'α -Adducin gene promoter DNA methylation and the risk of essential hypertension', *Clinical and Experimental Hypertension*. Taylor & Francis, 00(00), pp. 1–5.

Bednarek, E. and Caroni, P. (2011) 'β-adducin is required for stable assembly of new synapses and improved memory upon environmental enrichment', *Neuron*, 69(6), pp. 1132–1146.

Bennett, V. and Baines, A. J. (2001) 'Spectrin and Ankyrin-Based Pathways: Metazoan Inventions for Integrating Cells Into Tissues', *Physiol Rev*, 81(3), pp. 1353–1392.

Bhatia, H. S. *et al.* (2016) 'Rice bran derivatives alleviate microglia activation: possible involvement of MAPK pathway', *Journal of Neuroinflammation*, 13(1), p. 148.

Blank, T. *et al.* (2018) 'Early Microglia Activation Precedes Photoreceptor Degeneration in a Mouse Model of CNGB1-Linked Retinitis Pigmentosa', *Frontiers in Immunology*, 8.

Block, M. L. and Hong, J. S. (2005) 'Microglia and inflammation-mediated neurodegeneration: Multiple triggers with a common mechanism', *Progress in Neurobiology*, 76(2), pp. 77–98.

Bosia, M. *et al.* (2016) 'ADDing a piece to the puzzle of cognition in schizophrenia', *European Journal of Medical Genetics*. Elsevier Masson SAS, 59(1), pp. 26–31.

Bringmann, A. *et al.* (2006) 'Müller cells in the healthy and diseased retina', *Progress*

in Retinal and Eye Research, 25(4), pp. 397–424.

Van Buskirk, E. M. (1989) 'The anatomy of the limbus', *Eye (London, England)*, 3 (Pt 2), pp. 101–108.

Cairns, N. J., Lee, V. M. Y. and Trojanowski, J. Q. (2004) 'The cytoskeleton in neurodegenerative diseases', *Journal of Pathology*, pp. 438–449.

Campellone, K. G. and Welch, M. D. (2010) 'A nucleator arms race: Cellular control of actin assembly', *Nature Reviews Molecular Cell Biology*, pp. 237–251.

Campos, E. J., McVey, C. E. and Astier, Y. (2016) 'Stochastic Detection of MPSA-Gold Nanoparticles Using a α-Hemolysin Nanopore Equipped with a Noncovalent Molecular Adaptor', *Analytical Chemistry*, 88(12), pp. 6214–6222.

Cepko, C. (2014) 'Intrinsically different retinal progenitor cells produce specific types of progeny', *Nature Reviews Neuroscience*. Nature Publishing Group, 15(9), pp. 615–627.

Cepko, C. L. (2015) 'The Determination of Rod and Cone Photoreceptor Fate', *Annual Review of Vision Science*, 1(1), pp. 211–234.

Cholkar, K. *et al.* (2013) *Eye: Anatomy, physiology and barriers to drug delivery*, *Ocular Transporters and Receptors: Their Role in Drug Delivery*.

Cole, D. F. (1982) *Adler's Physiology of the Eye: Clinical Application*, The British journal of ophthalmology.

Coleman, J. E. and Semple-Rowland, S. L. (2005) 'GC1 deletion prevents light-dependent arrestin translocation in mouse cone photoreceptor cells', *Investigative Ophthalmology and Visual Science*, 46(1), pp. 12–16.

Coles, C. H. and Bradke, F. (2015) 'Coordinating Neuronal Actin-Microtubule Dynamics', *Current Biology*. Elsevier Ltd, 25(15), pp. R677–R691.

Coorey, N. J. *et al.* (2012) 'The role of glia in retinal vascular disease', *Clinical and Experimental Optometry*, 95(3), pp. 266–281.

Cunha-Vaz, J. (2009) 'The Blood–Retinal Barrier in Retinal Disease', *European Ophthalmic Review*, 03(02), p. 105.

Cunha-Vaz, J. G. (2004) 'The blood-retinal barriers system. Basic concepts and clinical evaluation', *Experimental Eye Research*, pp. 715–721.

Deitch, A. D. and Murray, M. R. (1956) 'The Nissl substance of living and fixed spinal ganglion cells. I. A phase contrast study.', *The Journal of biophysical and biochemical cytology*, 2(4), pp. 433–44.

Dong, L. *et al.* (1995) '35H, a sequence isolated as a protein kinase C binding protein, is a novel member of the adducin family', *Journal of Biological Chemistry*, 270(43), pp. 25534–25540.

Duan, W. R. *et al.* (2003) 'Comparison of immunohistochemistry for activated caspase-3 and cleaved cytokeratin 18 with the TUNEL method for quantification of apoptosis in histological sections of PC-3 subcutaneous xenografts', *The Journal of Pathology*, 199(2), pp. 221–228.

DuVal, M. and Allison, Wt. (2017) 'Impacts of the retinal environment and photoreceptor type on functional regeneration', *Neural Regeneration Research*, 12(3), p. 376.

Ebrahimi, V. *et al.* (2014) 'Histochemical study of retinal photoreceptors development during pre- and postnatal period and their association with retinal pigment epithelium', *Iranian Journal of Basic Medical Sciences*, (17), pp. 483–489.

Eitzen, U. V. *et al.* (1998) 'Microglia and the development of spongiform change in Creutzfeldt-Jakob disease', *Journal of Neuropathology and Experimental Neurology*, 57(3), pp. 246–256.

Erisir, A. *et al.* (1999) 'Function of Specific K^+ Channels in Sustained High-Frequency Firing of Fast-Spiking Neocortical Interneurons', *J Neurophysiol*, 82(5), pp. 2476–2489.

Euler, T. *et al.* (2014) 'Retinal bipolar cells: Elementary building blocks of vision', *Nature Reviews Neuroscience*. Nature Publishing Group, 15(8), pp. 507–519.

Fernández-Sánchez, L. *et al.* (2015) 'Astrocytes and Müller Cell Alterations During Retinal Degeneration in a Transgenic Rat Model of Retinitis Pigmentosa', *Frontiers in Cellular Neuroscience*, 9(December), pp. 1–16.

Fernández-Sánchez, L. L. *et al.* (2014) 'Loss of outer retinal neurons and circuitry alterations in the DBA/2J mouse', *Investigative Ophthalmology and Visual Science*, 55(9), pp. 6059–6072.

Fitzgibbon, T. (1997) ‘The human fetal retinal nerve fiber layer and optic nerve head: A DiI and DiA tracing study’, *Visual Neuroscience*. Cambridge University Press, 14(03), pp. 433–447.

Flynn, K. C. (2013) ‘The cytoskeleton and neurite initiation’, *Bioarchitecture*, pp. 86–109.

Fowler, L. *et al.* (1998) ‘Transformation-sensitive changes in expression, localization, and phosphorylation of adducins in renal proximal tubule epithelial cells’, *Cell growth & differentiation : the molecular biology journal of the American Association for Cancer Research*, 9(2), pp. 177–184.

Franze, K. *et al.* (2007) ‘Müller cells are living optical fibers in the vertebrate retina’, *Proceedings of the National Academy of Sciences*, 104(20), pp. 8287–8292.

Fukata, Y. *et al.* (1999) ‘Phosphorylation of adducin by Rho-kinase plays a crucial role in cell motility.’, *The Journal of cell biology*, 145(2), pp. 347–361.

Gallo, G. (2013) ‘More than one ring to bind them all: Recent insights into the structure of the axon’, *Developmental Neurobiology*, 73(11), pp. 799–805.

Galloway, N. R. *et al.* (2016) *Common eye diseases and their management, fourth edition*, Springer.

Gao, Y. *et al.* (2015) ‘Totarol prevents neuronal injury in vitro and ameliorates brain ischemic stroke: Potential roles of Akt activation and HO-1 induction’, *Toxicology and Applied Pharmacology*, 289(2), pp. 142–154.

Garden, G. A. and Möller, T. (2006) ‘Microglia biology in health and disease’, *Journal of Neuroimmune Pharmacology*, 1(2), pp. 127–137.

Gardner, K. and Bennett, V. (1986) ‘A new erythrocyte membrane-associated protein with calmodulin binding activity. Identification and purification’, *Journal of Biological Chemistry*, 261(3), pp. 1339–1348.

Gehrig, A. *et al.* (2007) ‘Genome-wide expression profiling of the retinoschisin-deficient retina in early postnatal mouse development.’, *Investigative ophthalmology & visual science*, 48(2), pp. 891–900.

Gerhardinger, C. *et al.* (2005) ‘Expression of acute-phase response proteins in retinal Müller cells in diabetes’, *Investigative Ophthalmology and Visual Science*,

46(1), pp. 349–357.

Gilligan, D. M. *et al.* (1999) ‘Targeted disruption of the beta adducin gene (Add2) causes red blood cell spherocytosis in mice.’, *Proceedings of the National Academy of Sciences of the United States of America*, 96(19), pp. 10717–22.

Goel, M. *et al.* (2010) ‘Aqueous humor dynamics: a review.’, *The open ophthalmology journal*, 4, pp. 52–9.

Graeber, M. B. and Streit, W. J. (1990) ‘Microglia: Immune Network in the CNS’, *Brain Pathology*, pp. 2–5.

Greter, M. and Merad, M. (2013) ‘Regulation of microglia development and homeostasis’, *Glia*, 61(1), pp. 121–127.

Guduric-Fuchs, J. *et al.* (2009) ‘Immunohistochemical study of pig retinal development.’, *Molecular vision*, 15(April), pp. 1915–1928.

Hamdan, R. *et al.* (2012) ‘Optical coherence tomography: From physical principles to clinical applications’, *Archives of Cardiovascular Diseases*, pp. 529–534.

Hammarlund, M., Jorgensen, E. M. and Bastiani, M. J. (2007) ‘Axons break in animals lacking β-spectrin’, *Journal of Cell Biology*, 176(3), pp. 269–275.

Hanisch, U. K. (2002) ‘Microglia as a source and target of cytokines’, *GLIA*, pp. 140–155.

Hernandez, M. *et al.* (2009) ‘Immunohistochemical changes in rat retinas at various time periods of elevated intraocular pressure.’, *Molecular vision*, pp. 2696–709.

Hetier, E. *et al.* (1988) ‘Brain macrophages synthesize interleukin-1 and interleukin-1 mRNAs in vitro’, *Journal of Neuroscience Research*, 21(2–4), pp. 391–397.

Hildebrand, G. D. and Fielder, A. R. (2011) ‘Anatomy and physiology of the retina’, in *Pediatric Retina*, pp. 39–65.

Holopigian, K. *et al.* (1992) ‘A Comparison of Phoropic and Scotopic Electroretinogrophic Changes in Early Diabetic Refinoparhy’, *Investigative Ophthalmology*, 33(10), pp. 2773–2780.

Hu, J.-H. *et al.* (2003) ‘Protein kinase and protein phosphatase expression in amyotrophic lateral sclerosis spinal cord’, *Journal of Neurochemistry*, 85(2), pp. 432–442.

Huang, C.-C. and Chen, W. (2018) ‘Raman spectroscopic analysis of cataract lens: A compendious review’, *Applied Spectroscopy Reviews*. Taylor & Francis, 0(0), pp. 1–14.

Hughes, C. A. and Bennett, V. (1995) ‘Adducin: A physical model with implications for function in assembly of spectrin-actin complexes’, *Journal of Biological Chemistry*, 270(32), pp. 18990–18996.

Humason, Gretchen L. (1962) Animal Tissue Techniques. Freeman, San Francisco, Calif., *Science*, 137(3527), pp. 332–333.

Ito, D. *et al.* (1998) ‘Microglia-specific localisation of a novel calcium binding protein, Iba1’, *Molecular Brain Research*, 57(1), pp. 1–9.

Ito, D. *et al.* (2001) ‘Enhanced expression of Iba1, ionized calcium-binding adapter molecule 1, after transient focal cerebral ischemia in rat brain’, *Stroke*, 32(5), pp. 1208–1215.

Jaffe, G. J. and Caprioli, J. (2004) ‘Optical coherence tomography to detect and manage retinal disease and glaucoma’, *American Journal of Ophthalmology*, pp. 156–169.

Jeon, C. J., Strettoi, E. and Masland, R. H. (1998) ‘The major cell populations of the mouse retina’, *J Neurosci*, 18(21), pp. 8936–8946.

Johansson, U. E., Eftekhari, S. and Warfvinge, K. (2010) ‘A battery of cell- and structure-specific markers for the adult porcine retina’, *Journal of Histochemistry and Cytochemistry*, 58(4), pp. 377–389.

Johnson, M., McLaren, J. W. and Overby, D. R. (2017) ‘Unconventional aqueous humor outflow: A review’, *Experimental Eye Research*, pp. 94–111.

Joshi, R. *et al.* (1991) ‘Primary structure and domain organization of human alpha and beta adducin.’, *The Journal of cell biology*, 115(3), pp. 665–675.

Kapitein, L. C. and Hoogenraad, C. C. (2011) ‘Which way to go? Cytoskeletal organization and polarized transport in neurons’, *Molecular and Cellular Neuroscience*. Elsevier Inc., 46(1), pp. 9–20.

Karlstetter, M., Ebert, S. and Langmann, T. (2010) ‘Microglia in the healthy and degenerating retina: Insights from novel mouse models’, *Immunobiology*. Elsevier,

215(9–10), pp. 685–691.

Kemmler, R. *et al.* (2014) 'Differential regulation of cone calcium signals by different horizontal cell feedback mechanisms in the mouse retina.', *The Journal of neuroscience : the official journal of the Society for Neuroscience*, 34(35), pp. 11826–43.

Kettenmann, H., Banati, R. and Walz, W. (1993) 'Electrophysiological behavior of microglia', *Glia*, 7(1), pp. 93–101.

Kim, S. U. and de Vellis, J. (2005) 'Microglia in health and disease', *Journal of Neuroscience Research*, 81(3), pp. 302–313.

Klaassen, I., Van Noorden, C. J. F. and Schlingemann, R. O. (2013) 'Molecular basis of the inner blood-retinal barrier and its breakdown in diabetic macular edema and other pathological conditions', *Progress in Retinal and Eye Research*. Elsevier Ltd, 34, pp. 19–48.

Kokona, D., Ebneter, A. and Zinkernagel, M. (2017) 'Activation of retinal microglia and accumulation of sub-retinal fluid after systemic challenge with Lipopolysaccharide in mice', *Acta Ophthalmologica*, 95.

Kolb, H., Fernandez, E. and Nelson, R. (1995) *Webvision*, *Webvision: The Organization of the Retina and Visual System*.

Kreutzberg, G. W. (1996) 'Microglia: A sensor for pathological events in the CNS', *Trends in Neurosciences*, pp. 312–318.

Krieger, C. *et al.* (2016) 'Adducin at the Neuromuscular Junction in Amyotrophic Lateral Sclerosis: Hanging on for Dear Life', *Frontiers in Cellular Neuroscience*, 10(January), pp. 1–12.

Kruer, M. C. *et al.* (2013) 'Mutations in gamma adducin are associated with inherited cerebral palsy', *Annals of Neurology*, 74(6), pp. 805–814.

Kugelmann, D., Waschke, J. and Radeva, M. Y. (2015) 'Adducin is involved in endothelial barrier stabilization', *PLoS ONE*, 10(5), pp. 1–16.

Kuhlman, P. A. *et al.* (1996) 'A New Function for Adducin', *The Journal of Biological Chemistry*, 271(14), pp. 7986–91.

Kur, J., Newman, E. A. and Chan-Ling, T. (2012) 'Cellular and physiological

mechanisms underlying blood flow regulation in the retina and choroid in health and disease', *Progress in Retinal and Eye Research*, pp. 377–406.

Lechner, J., O'Leary, O. E. and Stitt, A. W. (2017) 'The pathology associated with diabetic retinopathy', *Vision Research*. Elsevier Ltd, 139, pp. 7–14.

Leite, S. C. *et al.* (2016) 'The Actin-Binding Protein α-Adducin Is Required for Maintaining Axon Diameter', *Cell Reports*, 15(3), pp. 490–498.

Leite, S. C. and Sousa, M. M. (2016) 'The neuronal and actin commitment: Why do neurons need rings?', *Cytoskeleton*, 73(9), pp. 424–434.

Letourneau, P. C. (2009) 'Actin in Axons: Stable Scaffolds and Dynamic Filaments', in, pp. 265–290.

Li, X. L. and Bennett, V. (1995) 'Identification Of the Spectrin Subunit and Domains Required For Formation Of Adducin/Spectrin/Actin Complexes', *Molecular Biology Of The Cell*, 6(SS), p. 1564.

Li, X., Matsuoka, Y. and Bennett, V. (1997) 'Adducin preferentially recruits spectrin to fast-growing ends of actin filaments in a complex requiring the MARCKS related domain and an oligomerization domain', *Molecular Biology Of The Cell*, 8(SS), p. 1591.

Liu, W., Tang, Y. and Feng, J. (2011) 'Cross talk between activation of microglia and astrocytes in pathological conditions in the central nervous system', *Life Sciences*. Elsevier Inc., 89(5–6), pp. 141–146.

Liu, X. *et al.* (2013) 'Calcium channels in rat horizontal cells regulate feedback inhibition of photoreceptors through an unconventional GABA- and pH-sensitive mechanism', *Journal of Physiology*, 591(13), pp. 3309–3324.

Lukinavičius, G. *et al.* (2014) 'Fluorogenic probes for live-cell imaging of the cytoskeleton', *Nature Methods*, 11(7), pp. 731–733.

MacGillivray, T. J. *et al.* (2014) 'Retinal imaging as a source of biomarkers for diagnosis, characterization and prognosis of chronic illness or long-term conditions', *British Journal of Radiology*, 87(1040).

MacNeil, M. A. and Masland, R. H. (1998) 'Extreme diversity among amacrine cells: Implications for function', *Neuron*, 20(5), pp. 971–982.

Madeira, M. H. *et al.* (2015) ‘Contribution of microglia-mediated neuroinflammation to retinal degenerative diseases’, *Mediators of Inflammation*, 2015.

Martins*, J. (2014)* 'Modulation of retinal ganglion cell functions and implications for neuroprotection', (Doctoral dissertation). Available at: https://estudogeral.sib.uc.pt//handle/10316/26530.

Masland, R. H. (2012) ‘The tasks of amacrine cells’, *Visual Neuroscience*, pp. 3–9.

Matsuoka, Y., Hughes, C. A. and Bennett, V. (1996) ‘Adducin regulation. Definition of the calmodulin-binding domain and sites of phosphorylation by protein kinases A and C’, *Journal of Biological Chemistry*, 271(41), pp. 25157–25166.

Matsuoka, Y., Li, X. and Bennett, V. (1998) ‘Adducin is an *in vivo* substrate for protein kinase C: Phosphorylation in the MARCKS-related domain inhibits activity in promoting spectrin-actin complexes and occurs in many cells, including dendritic spines of neurons’, *Journal of Cell Biology*, 142(2), pp. 485–497.

Matsuoka, Y., Li, X. and Bennett, V. (2000) ‘Adducin: structure, function and regulation.’, *Cellular and molecular life sciences : CMLS*, 57(6), pp. 884–895.

McMurray, C. (2000) 'Neurodegeneration: diseases of the cytoskeleton?' *Cell Death & Differentiation*, 7(10), pp. 861-865.

Melloni, B. J. (1971) ‘How the retina works.’, *American Family Physician*, 4(2), p. 81.

Miller, R. F. and Dowling, J. E. (1970) ‘Intracellular responses of the Müller (glial) cells of mudpuppy retina: their relation to b-wave of the electroretinogram.’, *Journal of Neurophysiology*, 33(3), pp. 323–341.

Minghetti, L. and Levi, G. (1998) ‘Microglia as effector cells in brain damage and repair: Focus on prostanoids and nitric oxide’, *Progress in Neurobiology*, 54(1), pp. 99–125.

Mitchell, L. and Grimmer, P. (2013) ‘Causes, Complications and Treatment of a Red Eye’, *Best Practice Journal*, 54, pp. 8–21.

Miura, G. *et al.* (2016) ‘Effects of cataracts on flicker electroretinograms recorded with RETeval^{TM} system: New mydriasis-free ERG device Retina’, *BMC Ophthalmology*, 16(1).

Morgan, J. and Wong, R. (2007) ‘Development of Cell Types and Synaptic

Connections in the Retina', in *Webvision: The Organization of the Retina and Visual System*.

Müller, B. *et al.* (2017) 'Organotypic Cultures of Adult Mouse Retina: Morphologic Changes and Gene Expression', *Investigative Opthalmology & Visual Science*, 58(4), p. 1930.

Naydenov, N. G. and Ivanov, A. I. (2011) 'Spectrin-adducin membrane skeleton: A missing link between epithelial junctions and the actin cytoskeletion?', *BioArchitecture*, 1(4), pp. 186–191.

Newman, E. A. (2010) 'Retinal glia', in *Encyclopedia of Neuroscience*, pp. 225–232.

Newman, E. and Reichenbach, A. (1996) 'The Müller cell: A functional element of the retina', *Trends in Neurosciences*, 19(8), pp. 307–312.

Pielage, J. *et al.* (2011) 'Hts/adducin controls synaptic elaboration and elimination', *Neuron*, 69(6), pp. 1114–1131.

Pournaras, C. J. *et al.* (2008) 'Regulation of retinal blood flow in health and disease', *Progress in Retinal and Eye Research*, 27(3), pp. 284–330.

Presta, M. *et al.* (1995) 'Expression of basic fibroblast growth factor and its receptors in human fetal microglia cells', *International Journal of Developmental Neuroscience*, 13(1), pp. 29–39.

Provis, J. M. *et al.* (2005) 'Anatomy and development of the macula: Specialisation and the vulnerability to macular degeneration', *Clinical and Experimental Optometry*, pp. 269–281.

Puller, C. *et al.* (2017) 'Dendritic stratification differs among retinal OFF bipolar cell types in the absence of rod photoreceptors', *PLoS ONE*, 12(3), pp. 1–11.

Purves, D. *et al.* (2004) *Neuroscience, Third Edition*, Sunderland.

Quina, L. A. (2005) 'Brn3a-Expressing Retinal Ganglion Cells Project Specifically to Thalamocortical and Collicular Visual Pathways', *Journal of Neuroscience*, 25(50), pp. 11595–11604.

Reese, B. E. (2005) 'Afferents and Homotypic Neighbors Regulate Horizontal Cell Morphology, Connectivity, and Retinal Coverage', *Journal of Neuroscience*, 25(9), pp. 2167–2175.

Robberecht, W. and Philips, T. (2013) 'The changing scene of amyotrophic lateral sclerosis', *Nature Reviews Neuroscience*, pp. 248–264.

Robledo, R. F. *et al.* (2008) 'Targeted deletion of alpha-adducin results in absent beta- and gamma-adducin, compensated hemolytic anemia, and lethal hydrocephalus in mice', *Blood*, 112(10), pp. 4298–4307.

Robledo, R. F. *et al.* (2012) 'Strain-specific hyperkyphosis and megaesophagus in Add1 null mice', *Genesis*, 50(12), pp. 882–891.

Rogers, J. *et al.* (2002) 'Microglia and inflammatory mechanisms in the clearance of amyloid β peptide', *Glia*, 40(2), pp. 260–269.

Rosolen, S. G. *et al.* (2008) 'Retinal electrophysiology for toxicology studies: Applications and limits of ERG in animals and ex vivo recordings', *Experimental and Toxicologic Pathology*, 60(1), pp. 17–32.

Roy, S. (2016) 'Waves, rings, and trails: The scenic landscape of axonal actin', *Journal of Cell Biology*, 212(2), pp. 131–134.

Saijo, K. and Glass, C. K. (2011) 'Microglial cell origin and phenotypes in health and disease', *Nature Reviews Immunology*, pp. 775–787.

Sanchez-Tocino, H. *et al.* (2002) 'Retinal Thickness Study with Optical Coherence Tomography in Patients with Diabetes', *Invest. Ophthalmol. Vis. Sci.*, 43(5), pp. 1588–1594.

Santiago, A. R. *et al.* (2014) 'Role of Microglia Adenosine A 2A Receptors in Retinal and Brain Neurodegenerative Diseases', *Mediators of Inflammation*, 2014, pp. 1–13.

Schiller, P. H. (2010) 'Parallel information processing channels created in the retina', *Proceedings of the National Academy of Sciences*, 107(40), pp. 17087–17094.

Shan, X. *et al.* (2005) 'Increased phospho-adducin immunoreactivity in a murine model of amyotrophic lateral sclerosis', *Neuroscience*, 134(3), pp. 833–846.

Siggers, J. H. and Ethier, C. R. (2012) 'Fluid Mechanics of the Eye', *Annual Review of Fluid Mechanics*, 44(1), pp. 347–372.

Sivakumar, V. *et al.* (2011) 'Retinal ganglion cell death is induced by microglia derived pro-inflammatory cytokines in the hypoxic neonatal retina', *Journal of*

Pathology, 224(2), pp. 245–260.

Snytnikova, O. A. *et al.* (2017) 'Quantitative metabolomic analysis of the human cornea and aqueous humor', *Metabolomics*. Springer US, 13(12), pp. 1–9.

Squire, L., and Bloom, F. (2012). Fundamental Neuroscience. San Diego: Elsevier Science.

Stevens, R. J. and Littleton, J. T. (2011) 'Synaptic growth: Dancing with adducin', *Current Biology*, 21(10).

Stewart, E. and Shen, K. (2015) 'STORming towards a clear picture of the cytoskeleton in neurons', *eLife*, 2015(4).

Stiess, M. and Bradke, F. (2010) 'Neuronal polarization: The cytoskeleton leads the way', *Dev Neurobiol*, 71(6), pp. 430–444.

Stockton, R. a and Slaughter, M. M. (1989) 'B-wave of the electroretinogram. A reflection of ON bipolar cell activity.', *The Journal of General Physiology*, 93(1), pp. 101–122.

Stöhr, H., Stojic, J. and Weber, B. H. (2003) 'Cellular localization of the MPP4 protein in the mammalian retina', *Investigative Ophthalmology & Visual Science*, 44(12), pp. 5067–5074.

Streit, W. J. (2002) 'Microglia as neuroprotective, immunocompetent cells of the CNS', *GLIA*, pp. 133–139.

Strettoi, E. *et al.* (2002) 'Morphological and functional abnormalities in the inner retina of the rd/rd mouse', *J Neurosci*, 22(13), pp. 5492–5504.

Szalay, G. *et al.* (2016) 'Microglia protect against brain injury and their selective elimination dysregulates neuronal network activity after stroke', *Nature Communications*, 7.

Thoreson, W. B. and Mangel, S. C. (2012) 'Lateral interactions in the outer retina', *Progress in Retinal and Eye Research*, pp. 407–441.

Torielli, L. *et al.* (2008) 'α-Adducin mutations increase Na/K pump activity in renal cells by affecting constitutive endocytosis: implications for tubular Na reabsorption.', *American journal of physiology. Renal physiology*, 295(2), pp. F478-87.

Tremblay, M. È. and Sierra, A. (2014) *Microglia in health and disease*, Springer

Tsai, Y. *et al.* (2014) 'Ocular changes in TGF344-AD rat model of Alzheimer's disease', *Investigative Ophthalmology and Visual Science*, 55(1), pp. 523–534.

Tura, A. *et al.* (2009) 'Efficacy of Rho-kinase inhibition in promoting cell survival and reducing reactive gliosis in the rodent retina', *Investigative Ophthalmology and Visual Science*, 50(1), pp. 452–461.

Völgyl, B., Chheda, S. and Bloomfield, S. A. (2009) 'Tracer coupling patterns of the ganglion cell subtypes in the mouse retina', *Journal of Comparative Neurology*, 512(5), pp. 664–687.

Vecino, E. *et al.* (2016) 'Glia-neuron interactions in the mammalian retina', *Progress in Retinal and Eye Research*. Elsevier Ltd, 51, pp. 1–40.

Verma, R. and Pianta, M. J. (2009) 'The contribution of human cone photoreceptors to the photopic fl icker electroretinogram', *Journal of Vision*, 9(3), pp. 1–12.

Vukojevic, V. *et al.* (2012) 'A role for α-adducin (ADD-1) in nematode and human memory', *EMBO Journal*. Nature Publishing Group, 31(6), pp. 1453–1466.

Wachtmeister, L. (1998) 'Oscillatory potentials in the retina: What do they reveal', *Progress in Retinal and Eye Research*, 17(4), pp. 485–521.

Wang, L. *et al.* (2002) 'Immunohistologic evidence for retinal glial cell changes in human glaucoma', *Investigative Ophthalmology and Visual Science*, 43(4), pp. 1088–1094.

Wang, S. *et al.* (2010) 'Non-invasive stem cell therapy in a rat model for retinal degeneration and vascular pathology', *PLoS ONE*, 5(2).

Wässle, H. *et al.* (1998) 'Calcium-binding proteins in the retina of a calbindin-null mutant mouse', *Cell and Tissue Research*, 292(2), pp. 211–218.

Watson, N. V and Breedlove, S. M. (2012) 'The mind's machine: Foundations of brain and behavior.', *The mind's machine: Foundations of brain and behavior.*

Weber, B. H. F. and Langmann, T. (eds) (2013) *Retinal Degeneration*. Totowa, NJ: Humana Press (Methods in Molecular Biology).

Weinstein, J. R. *et al.* (2005) 'Unraveling thrombin's true microglia-activating potential: markedly disparate profiles of pharmaceutical-grade and commercial-grade thrombin preparations', *Journal of Neurochemistry*, 95(4), pp. 1177–1187.

Werblin, F. S. (2011) ‘The retinal hypercircuit: A repeating synaptic interactive motif underlying visual function’, *Journal of Physiology*, pp. 3691–3702.

Williams, L. J. and Abdi, H. H. (2010) ‘Fisher’s least significant difference (LSD) test’, *Encyclopedia of research design*, pp. 1–6.

Wu, S. M. (2010) ‘Synaptic organization of the vertebrate retina: General principles and species-specific variations: The friedenwald lecture’, *Investigative Ophthalmology and Visual Science*, 51(3), pp. 1264–1274.

Xiong, W. H. *et al.* (2015) ‘The effect of PKC-α on the light response of rod bipolar cells in the mouse retina’, *Investigative Ophthalmology and Visual Science*, 56(8), pp. 4961–4974.

Xu, K., Zhong, G. and Zhuang, X. (2013) ‘Actin, Spectrin, and Associated Proteins Form a Periodic Cytoskeletal.pdf’, *Science (New York, N.Y.)*, pp. 452–6.

Zalis, M. C., Johansson, S. and Englund-Johansson, U. (2017) ‘Immunocytochemical Profiling of Cultured Mouse Primary Retinal Cells’, *Journal of Histochemistry and Cytochemistry*, 65(4), pp. 223–239.

Zeiss, C. J. and Johnson, E. A. (2004) ‘Proliferation of microglia, but not photoreceptors, in the outer nuclear layer of the rd-1 mouse’, *Investigative Ophthalmology and Visual Science*, 45(3), pp. 971–976.

Zeng, H. Y. *et al.* (2005) ‘Identification of sequential events and factors associated with microglial activation, migration, and cytotoxicity in retinal degeneration in rd mice’, *Investigative Ophthalmology and Visual Science*, 46(8), pp. 2992–2999.

Zhang, K. *et al.* (2007) ‘Frequency spectrum and amplitude analysis of dark- and light-adapted oscillatory potentials in albino mouse, rat and rabbit’, *Documenta Ophthalmologica*, 115(2), pp. 85–93.

Zhong, G. *et al.* (2014) ‘Developmental mechanism of the periodic membrane skeleton in axons’, *eLife*, 3, pp. 1–21.